

Missing snowmelt runoff following drought explained by root-zone storage deficits

Dana A Lapiques^{1,2}, W Jesse Hahm², Daniella M Rempe³, David N Dralle¹

¹ Pacific Southwest Research Station, USDA Forest Service, Davis, CA, USA

² Department of Geography, Simon Fraser University, Burnaby, BC, Canada

³ University of Texas, Austin, Austin, TX, USA

This pre-print is not peer-reviewed. This pre-print was submitted to *PNAS*.

Missing snowmelt runoff following drought explained by root-zone storage deficits

Dana A Lapides^{a,b,1}, W Jesse Hahm^b, Daniella M Rempe^c, and David N Dralle^a

^aPacific Southwest Research Station, United States Forest Service, Davis, CA, USA; ^bDepartment of Geography, Simon Fraser University, Burnaby, BC, Canada; ^cUniversity of Texas, Austin, Austin, TX, USA

This manuscript was compiled on March 16, 2022

Water resources management in mountainous regions hinges on forecasting runoff during annual snowmelt periods. However, extreme droughts are altering snowpack-runoff relationships. The current megadrought in the Western United States provides a case in point: in 2021 in California, the historically reliable relationship between April 1 snowpack and runoff failed—much less streamflow arrived than was predicted. Several factors have been proposed to account for this ‘missing’ streamflow, including changes in: evapotranspiration, rainfall, snowmelt rate, and subsurface moisture conditions. Here, we use hydrologic data from 13 minimally disturbed basins and 6 water supply basins in the Sierra Nevada to demonstrate that the root-zone storage deficit (i.e., the net depletion of plant-accessible water from soil and weathered bedrock via evapotranspiration) is the dominant driver of snowmelt runoff reductions in years following drought. Transpiration in excess of precipitation in drought years generates large deficits that must be met prior to significant streamflow generation. We introduce a mass balance model that captures this effect to motivate model structures for forecasting models. By accounting for deficits in models for snowmelt runoff, overprediction of 2021 streamflow decreased from a total of $\approx 100\%$ to $< 12\%$ at study sites in the Sierra Nevada. Our findings indicate that the relationship between snowpack and runoff will evolve as plant ecosystems respond to climate change and alter subsurface water storage dynamics. Through this climatic transition, root-zone storage deficits will play an essential role in snowmelt runoff prediction, and this study provides a framework for adapting forecasting models with readily-available data.

Sierra Nevada | Forecasting | Water resources | Evapotranspiration | Snowpack

Introduction

Mountain snowpack is an essential water reservoir for 1.9 billion people globally (2). However, the accessibility of this water depends on how snowmelt runoff is generated. Historically, managers have relied on statistical relationships between snowpack and subsequent runoff for forecasting (3), but changes in climate can alter these relationships. Recently, following a severe drought in California, streamflow forecasts from historically reliable snowpack-runoff relationships (4) far exceeded actual streamflow (see for example, Figure 1a-b). This led scientists and the public alike (e.g., 5, 6) to wonder—where did the missing snowmelt go?

Previous work has proposed that shifts in streamflow generation from a given water input (snowpack) arise from differences in evapotranspiration (ET) due to changes in evaporative demand (7–9), snowmelt rate (10), and/or vegetation community (11–13). Antecedent moisture conditions have also been proposed to alter the relationship between water inputs

and resulting streamflow (e.g., 8, 14–16), including the role of rainfall inputs during the winter season and subsurface moisture conditions at the start of the winter season. Both of these factors can be tied to a form of runoff generation in which significant runoff is generated only after infiltrating water replenishes subsurface storage (17, 18). After the subsurface dries (typically through withdrawal of root-zone moisture by ET as shown in Figure 1d, 18–30), infiltrating water goes first to replenishing this moisture deficit and then towards generating streamflow. Less water input prior to snowmelt (i.e., winter rainfall) or more evapotranspiration during or prior to snowmelt (i.e., winter and spring ET) can limit how quickly the storage deficit is replenished—the precondition for significant streamflow generation. In this way, subsurface moisture conditions interact with above-ground factors to mediate runoff generation from snowpack.

Subsurface moisture deficits occur in soils as well as the underlying weathered bedrock, which can account for a large portion of root-zone water storage (20, 27, 31, 32). Although there have been advances in large-scale observation of shallow soil moisture conditions (33), deeper storage is less easy to monitor (26). Storage changes recorded by GRACE (34) are not finely resolved and include water storage effects (e.g., deep groundwater) that may not be relevant to the root-zone, and modeled subsurface water storage is contingent on the reliability of model parameterization and available soil textural databases, which cannot account for storage dynamics

Significance Statement

Essential water supply from snowpack may become more difficult to predict as the climate changes. Following a recent drought in California, the traditionally used model for snowmelt runoff failed. Here, we present a model that accounts for this model failure by incorporating the role of root-zone storage dynamics in the production of snowmelt runoff. Through transpiration, montane forests generate water storage deficits in the soils and weathered bedrock that comprise the root-zone. These deficits must be replenished by rain and snowmelt before significant runoff generation can occur. Overprediction of 2021 post-drought runoff in California can be primarily attributed to unprecedentedly large root-zone storage deficits. Adding a measure of deficit reduced 2021 streamflow prediction error from $\approx 100\%$ to $< 12\%$.

DND conceived of the study. DAL and DND formulated the hydrological model. DAL compiled data, conducted analyses, generated graphics, and wrote the initial manuscript. WJH and DND reviewed analysis code. All authors were involved in idea generation, significant manuscript revision, and review of the final manuscript.

The authors have no conflicts of interest to declare.

¹To whom correspondence should be addressed. E-mail: dlapides@sfu.ca

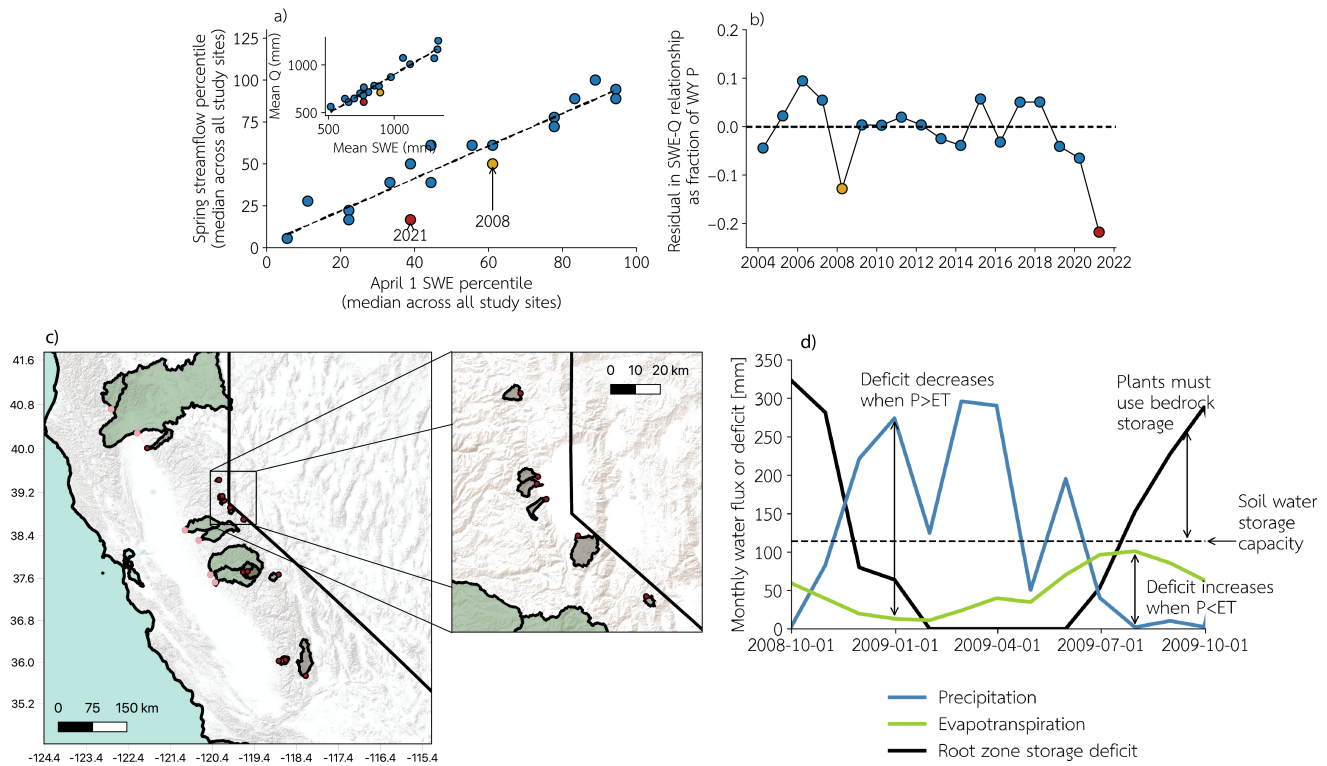


Fig. 1. (a) Linear relationship between April 1 snow water equivalent (SWE) and spring (April-July) streamflow summarized at 13 minimally disturbed sites as the relationship between median April 1 SWE percentile and median spring streamflow percentile for each year within the study period (2003-2021). This regression model is of a similar form to the one used by the California Department of Water Resources to produce streamflow forecasts. Inset shows the same plot for the mean value of April 1 SWE and spring streamflow among the 13 minimally disturbed sites. Points that fall above the dashed line are years where the linear model under-predicts streamflow, and points that lie below the line are years where the linear model over-predicts streamflow. 2021 and 2008 are highlighted as particularly large negative residuals. SWE data is from SNODAS (1). (b) Median residual in the SWE-spring streamflow relationship among the 13 minimally disturbed sites as a fraction of April 1 SWE. (c) Map of study watersheds in the Sierra Nevada. Red dots mark gage locations at watershed outlets for minimally disturbed sites shaded in grey, and pink dots for basins important for water supply shaded in green. (d) Explanatory plot for root-zone storage deficit for one water year. At the beginning of the wet season, the deficit decreases (storage fills up) to 0 and remains there until ET exceeds P again in the dry season, and the deficit grows until the beginning of the next wet season. Deficits in excess of the soil water storage capacity indicate plant use of water stored below soil in weathered bedrock.

46 in underlying bedrock (35).

47 An alternative approach for estimating runoff-mediating
 48 subsurface moisture conditions is to track the balance between
 49 fluxes entering and exiting the root-zone. Spatially distributed,
 50 running, near real-time plant-driven water storage dynamics
 51 throughout both soil and bedrock can thus be quantified from
 52 precipitation and ET timeseries (36–38). Considering storage
 53 deficits in runoff prediction (39) or as a harbinger of drought
 54 (40, 41) is not new, but the widespread availability of distributed
 55 and increasingly reliable ET, precipitation (36), snow
 56 cover (37), and snow water equivalent (SWE) datasets now
 57 make it possible to monitor deficits in mountainous regions at
 58 large scales.

59 In this study, we introduce a mass-balance model for
 60 snowmelt driven runoff in a Mediterranean environment (wet
 61 winter, dry growing season) that explicitly incorporates the
 62 root-zone water storage deficit to explore the following hypothesized
 63 explanations for snowmelt runoff reduction (see Figure
 64 2 for a schematic):

- 65 1. Less rainfall fell than usual during the winter or spring
- 66 2. Snowmelt rate was slower than usual
- 67 3. Evaporative demand was higher than usual during the
 68 winter

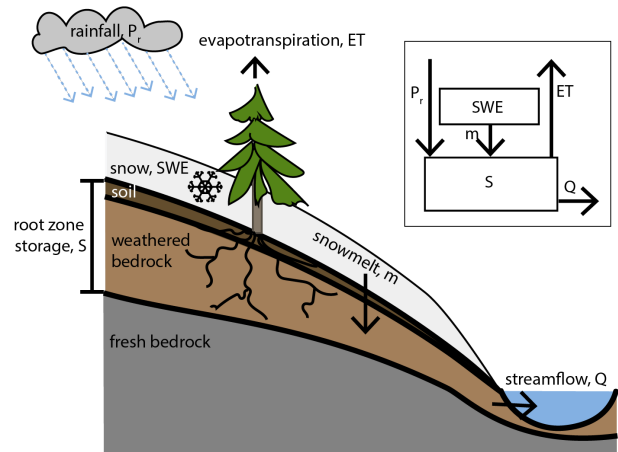


Fig. 2. Conceptual hillslope diagram of mountain hydrology. Thin soils cover a deep, weathered bedrock zone that plants may access throughout the dry season. Snow accumulates during the winter and melts into the subsurface, while rain directly replenishes the subsurface. Evapotranspiration reduces water in storage, and streamflow is generated once a subsurface storage deficit is replenished. The inset diagram shows the two modeled water reservoirs (snow and root-zone storage) and fluxes (rainfall, snowmelt, evapotranspiration, and streamflow).

- 69 4. Evaporative demand was higher than usual during the
70 spring
- 71 5. The root-zone water storage deficit at the start of the wet
72 season was larger than usual.

73 We validate our mass balance model against observed spring
74 streamflow at 13 minimally disturbed sites in the Sierra Nevada
75 (see the ‘Materials and methods’ section for more details), and
76 then develop a multiple linear regression model to quantify
77 which drivers have the largest impact on snowmelt runoff.
78 Based on results from the multiple linear regression analysis,
79 we quantify improvement in snowmelt runoff forecasts
80 in 2021 at 13 minimally disturbed watersheds as well as 6
81 watersheds important for California’s water supply. While we
82 specifically explore the fate of the ‘missing’ 2021 snowmelt
83 runoff in California, our goal is to understand how subsurface
84 water storage dynamics—in combination with other previously
85 studied mechanisms—inform forecasting of snowmelt runoff
86 in general.

87 **Results**

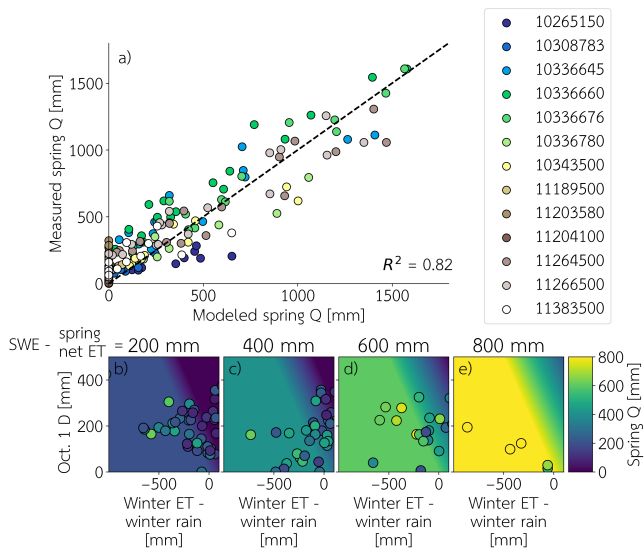


Fig. 3. (a) Comparison between measured spring streamflow at minimally disturbed study sites and predicted streamflow based on Equation 1. Legend refers to USGS streamgauge ID. (b-e) Heatmaps showing how modeled streamflow varies based on each model parameter. Within each panel: winter ET - winter rain increases moving right, and October 1 deficit increases vertically. Moving to the right between panels, April 1 SWE - (spring ET - spring rain) increases. Points plotted on heatmaps represent a single water year for a study site and are colored by measured spring streamflow. Points are plotted on the heatmaps if $SWE - ET_{net} - N_{melt}$ is within 100 mm of the value labeled for each panel.

88 The mass balance model of root-zone storage (Equation 1;
89 see Materials and Methods for model description) accurately
90 predicts measured spring streamflow ($R^2 = 0.84$ for one-to-
91 one line, see Figure 3a) at 13 minimally disturbed sites in
92 the Sierra Nevada (grey sites in Figure 1c). Panels b-e plot
93 these same predictions, showing scatter points colored by
94 actual spring streamflow against heatmaps generated from the
95 mass balance model. Good model performance despite a lack of
96 tunable parameters suggests that the model captures the
97 primary mechanisms for spring streamflow generation at the
98 study sites.

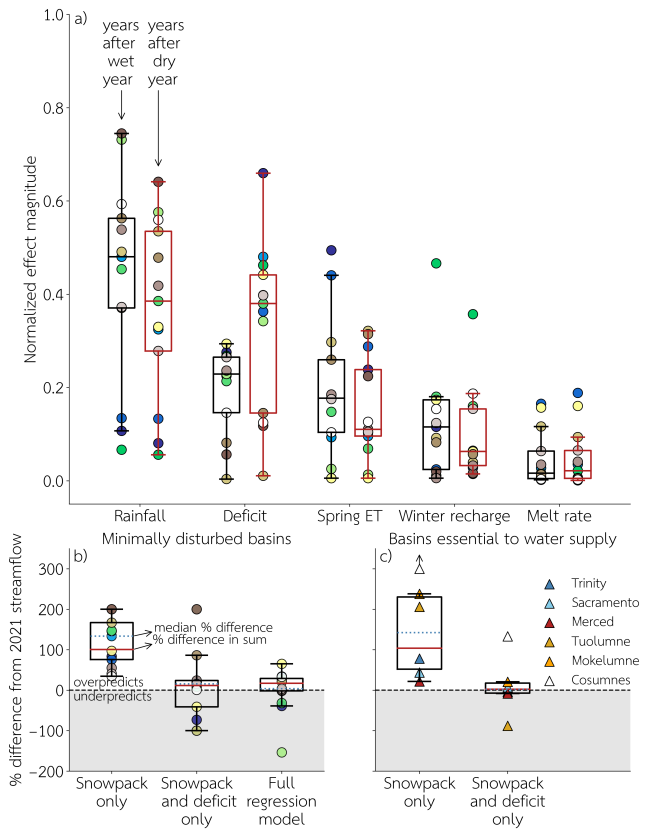


Fig. 4. a) Normalized effect magnitude of each variable included in the multiple linear regression for snowmelt runoff at all sites, comparing the set of years following wet years to years following dry years during the study period. Snowpack is consistently the most important variable and is excluded from this plot. Variable names are described for the water balance feature they represent, but rainfall, deficit, spring net ET, and winter recharge are relative to water year precipitation in the model to reduce correlation among variables, and melt rate is relative to spring net ET. Box and whisker plot shows median value across all sites. Effect size is the coefficient for a given variable multiplied by the median absolute value of the variable for years following wet (black) or dry (red) years. Normalization is achieved by scaling the effect sizes for each site so that their absolute values sum to 1, and the magnitude of these normalized values is reported. Panels b) and c) show performance of regression models at 13 minimally disturbed sites (b) and 6 basins important for California’s water supply (c) for the year 2021. A linear regression model using only April 1 SWE overpredicts the total 2021 spring streamflow at all minimally disturbed sites by 100% (median 134%), while the full linear regression model or a model using April 1 SWE and October deficit as a fraction of winter precipitation overpredicts the total by 17 or 12% (median of 15 or 4%), respectively. At the 6 basins important for California’s water supply, a linear regression using only April 1 SWE overpredicts median streamflow by 143%, versus 2% with a model using April 1 SWE and October deficit. Legend for panels a) and b) is the same as for Figure 3a.

root-zone storage deficit is important for determining runoff from snowpack. We regressed spring runoff (April-July, proxy for snowmelt runoff) on the variables identified in the storage-based modeling framework (Equation 2) at the 13 minimally disturbed sites to quantitatively rank the importance of different physical drivers of snowmelt runoff generation during years following both wet (above 75th percentile of annual precipitation) and dry (below 25th percentile of annual precipitation) years (Figure 4a). Model outcomes in both wet and dry years are most sensitive to snowpack, followed by rainfall since the amount of precipitation is the first-order control on snowmelt runoff. Rainfall, however, does not explain significantly lower model performance in years following wet versus dry years (median difference of 0.18 in R^2 , see Supplemental Information

Table 4 for site-specific details) since the effect size is similar. In contrast, the effect size of the deficit is substantially larger following dry years than wet years so that the deficit is as important as rainfall following dry years. In fact, the deficit is the only parameter that shows a substantial difference in effect size following dry years, suggesting that large deficits generated during dry years play an essential role in reducing snowmelt runoff in the following year. See Supplemental Tables 3 and 4 for effect sizes for all variables at all sites on wet and dry years.

With rare exceptions, the sign for each effect size matches the expected sign based on hypothesized model mechanisms at all sites (see Supplemental Table 3), providing further evidence for the proposed conceptual framework. No more than one site shows an unexpected sign for any parameter except for the melt rate, which has an unexpected sign at 4 sites. Given the melt rate's small effect sizes and unexpected effect signs, we conclude melt rate is relatively insignificant in comparison to other explanatory variables. The median R^2 value for multiple linear regression models across the study sites is 0.93.

We also trained a single random forest model to predict spring streamflow at all sites based on the same set of input parameters (model performance $R^2 = 0.98$) since a linear model may not account for complex interactions between the hydrologic processes used in the regression. Results from the random forest analysis also support the hypothesized mechanisms, and contribution of parameters to model outputs as measured by feature importance confirms that October 1 deficit and spring net ET are important drivers of snowmelt runoff, whereas the melt rate is less important. See Supplemental Information S6 for more details.

Using deficits increases predictive power of forecasting models. A linear regression model using only snowpack (Figure 1a) replicates the 2021 "missing" streamflow phenomenon with a similar magnitude of error in 2021 (4). By adding a term representing the deficit (linear regression using only snowpack and deficit), model performance improves to a median of $R^2 = 0.85$, a median improvement of 0.05 over a model using only snowpack. For site-specific details, see Supplemental Table 3.

When focusing on anomalous years such as the 2021 water year, gains in model performance are substantially larger than the modest improvement in R^2 would suggest (See Supplemental Information Figure S4 for details on improved model performance on a year with underprediction). Figure 4b shows predictions for 2021 streamflow at the minimally disturbed sites using the full multiple linear regression model, snowpack and deficit only, and snowpack only. Each regression model is trained on data from the full study period. Using only snowpack, the model over-predicts the 2021 total streamflow from all sites by 100%. Using the full regression model, total streamflow is only over-predicted by 17%, and with snowpack and deficit it is over-predicted by only 12%. For each site, the median overprediction using a regression model with only snowpack is 134%, with the full regression model 4%, and with snowpack and deficit 15%.

We tested our model on minimally disturbed basins. However, given that the deficit is calculated using remotely-sensed evapotranspiration, it should be sensitive to spatial variation in land-cover or forms of disturbance, such as fire, that are known to impact patterns of plant water use (42–45). This

suggests our model may be applicable to larger and more complex basins. We therefore also applied the model to six watersheds central to California's water supply (green basins in Figure 1c and Supplemental Information S1 for additional site information). As shown in Figure 4c, adding a term to a linear regression model to represent the deficit improves error in prediction of 2021 streamflow from a total of 104% to 2% overprediction or a median of 143% to 2%. Therefore, incorporating the root-zone storage deficit into models for spring streamflow from snowpack substantially improves model performance for water resources-relevant forecasting, especially following dry years.

Discussion and conclusions

Large drought-induced root-zone storage deficits at the start of the 2021 wet season led to the "missing" streamflow phenomenon. Adding a term to describe root-zone storage deficit decreased total overprediction of 2021 snowmelt runoff in a linear regression model from a 100% to 12%, an essential improvement for water resources management. Among the terms indicated to be most important, only the October 1 deficit can be quantified prior to the snowmelt season for the purpose of improved snowmelt runoff forecasting.

Managers and researchers have long recognized the importance of subsurface moisture conditions for subsequent runoff (e.g., personal communication with Sean de Guzman, chief of the California Department of Water Resources Snow Surveys and Water Supply Forecasting Section, and 18–30, 39); however, incorporating root-zone water storage dynamics into forecasting presents a challenge. This is due to both the limited available data on water storage in weathered bedrock, as well as the challenge of understanding interactions between different drivers of root-zone dynamics. The presented model quantitatively captures the expected importance of subsurface moisture conditions for runoff forecasting, providing a low-complexity solution to the problem of runoff prediction (36, 37). The model captures snowmelt runoff well following dry years, which is essential given the projected increase in "whiplash" (alternation between extreme wet and dry years, 46). A further implication of our findings is that runoff generation in the Sierra is probably not dependent on infiltration-excess overland flow processes, which should be relatively insensitive to root-zone storage deficits (47). Instead, the agreement between the presented model and data supports the hypothesis that replenishment of root-zone storage deficits is required for significant runoff generation to occur, which is more consistent with saturation overland (48) or subsurface (49) flow generation mechanisms.

Climate change is impacting the reliability and predictability of water supply in many different ways, just one of which is post-drought reductions in expected snowmelt runoff. Root-zone storage deficits provide a means of monitoring changing conditions, but operationalizing deficits in real-time requires the development of frequently-updated, reliable, large-scale ET and P datasets. Multiple data products are being developed and tested in the community to support urgent needs for research and management applications, and the present study provides yet more motivation to continue honing these essential datasets.

Table 1. Table of notation.

Variable	Dimensions	Description
Q	L	Total runoff during snowmelt period
SWE	L	Snowpack at start of snowmelt period
P	L	Water year total precipitation
m	L/T	Snowmelt rate
ET_s	L/T	Mean spring ET rate
ET_w	L	Total winter ET
P_s	L/T	Mean spring rainfall rate
P_w	L	Total winter rainfall
ET_{net}	L/T	Spring ET rate - spring rainfall rate
N_{melt}	T	Duration of snowmelt period
D_{Oct1}	L	Deficit at start of wet season

Mass-balance snowmelt runoff model. Here we expand upon a stochastic hydrological model (50) that incorporates storage as a simple 1-d bucket to describe annual runoff dynamics and plant water availability in Mediterranean catchments. In the original model, precipitation P [L] contributes water to storage during the wet season, and evapotranspiration ET [L] removes water from storage primarily during the dry season. Streamflow is generated only if the subsurface storage reservoir is full. The root-zone is treated as a single storage reservoir representing a thin soil layer underlain by deep weathered bedrock (Figure 2), as is common in forested mountainous environments (27, 51–53). The model does not specify where water is stored within the root-zone or its energy state (e.g., saturated versus unsaturated). Nor does it mechanistically specify how groundwater produces streamflow at the hillslope-channel boundary, only that water input volumes in excess of the deficit generate flow in the stream.

In our model formulation, storage dynamics evolve annually over three hydrological seasons: a winter wet season when rain enters storage and snow accumulates, a snowmelt season when rain and snowmelt enter storage, and a dry summer season. ET draws from storage at different rates in each season. Starting at the beginning of the wet season, there is a deficit generated by the previous dry season that shrinks with water input during the winter wet season and snowmelt periods (Figure 1d). Once the deficit is reduced to 0, streamflow is generated. When ET exceeds snowmelt and rain in the spring, streamflow stops, and the deficit grows again until the start of the next wet season. Snowmelt runoff emerges as the net water input during the melt season (snowmelt and precipitation less ET) once the deficit has been met. This mass balance results in an expression for snowmelt runoff (Q [L]), in which each of the proposed factors that could impact the relationship between snowpack and streamflow appear as variables:

$$Q = \begin{cases} \text{if } P_w - ET_w > D_{Oct1} : \\ \quad \max(0, SWE - (ET_s - P_s)N_{melt}) \\ \text{otherwise:} \\ \quad \max(0, SWE - (ET_s - P_s)N_{melt} - \\ \quad \quad D_{Oct1} + (P_w - ET_w)) \end{cases} \quad [1]$$

Notation is defined in Table 1. Both conditions are bounded by zero since streamflow cannot be negative. A negative value for either condition indicates that water demand from ET exceeds water availability from rain and snowmelt, so streamflow must

be zero. In Equation 1, all of the hypotheses listed at the end of the introduction for missing snowmelt appear: (1) rain appears in ET_{net} , P_w , and P_s , (2) snowmelt rate appears in $N_{melt} = SWE/m$, (3) ET appears in ET_s and ET_w , and (4) the deficit appears as D_{Oct1} . For a full description of the model, see Supplemental Information S2 and S3.

We validated our mass balance model against observed spring streamflow at 13 minimally disturbed sites in the Sierra Nevada and then developed a multiple linear regression model to quantify which drivers have the largest impact on snowmelt runoff. Results of the multiple linear regression analysis were used to develop a model structure for an improved forecast model, which was tested at the 13 minimally disturbed watersheds as well as 6 watersheds important to California's water supply.

A regression model for snowmelt-driven runoff. We performed exploratory data analysis to determine which hypotheses listed at the end of the introduction best explain snowmelt runoff at the study sites (Figure 1c). See Supplemental Information S1 for details on study sites and site selection criteria, and Supplemental Information S5 for additional details on exploratory analysis. To determine which mechanisms have the most explanatory power for deviations from the snowpack-runoff relationship, we developed a multiple linear regression equation at each study site:

$$Q = C_1 SWE + C_2 \frac{D_{Oct1}}{P} + C_3 \frac{ET_{net} N_{melt}}{P} + C_4 \frac{ET_w - P_w}{P} + C_5 \frac{P_w + P_s}{P} + C_6 \frac{m}{ET_{net}} + C_7, \quad [2]$$

where C_1, \dots, C_7 are fitted parameters.

Each variable other than SWE is expressed as a fraction of water year precipitation (except for m/ET_{net}). Expressing variables relative to water year P strengthens the relationship between variables and residuals in the SWE - Q relationship, similar to the finding of Hahm et al. (50) that the ratio between water year P and storage, not storage alone, is important for determining hydrological outcomes. This normalization also has the effect of minimizing correlation between variables since many model variables are correlated with water year P . In Equation 2, $ET_{net} N_{melt}/P$ and $(ET_w - P_w)/P$ capture effects of variable ET (Hypotheses 3 and 4 in the conceptual runoff model section), $(P_w + P_s)/P$ captures effects of variable rainfall (Hypothesis 1), m/ET_{net} captures effects of variable snowmelt rate (Hypothesis 2), and D_{Oct1}/P captures effects of variable root-zone storage deficit (Hypothesis 4). We also used a random forest model to corroborate the findings of this regression approach; see Supplemental Information S6 for additional details.

Data sources and data processing. Details on site selection criteria for the 13 minimally disturbed basins and site characteristics for all study basins are found in Supplemental Information S1.

Streamflow data were obtained from the National Water Information System (NWIS, 54) using the package hydrofunctions (<https://hydrofunctions.readthedocs.io/en/master/>). Daily snow water equivalent was obtained using SNODAS (1). Precipitation data were obtained from PRISM (55). Evapotranspiration and temperature data were obtained from PML V2 (56–58) and MODIS (59). PRISM, MODIS, and PML V2

317 were accessed via the Google Earth Engine Python API (60).
 318 Evaporative stress index (ESI) data were obtained from Cli-
 319 mateServ (61–64). ESI provides a measure of ET anomalies
 320 over time using thermal satellite imagery. A higher ESI indi-
 321 cates a larger positive ET anomaly, whereas lower or negative
 322 values indicate depressed ET. For comparison with root-zone
 323 storage deficit, we included soil water storage capacity (65) as
 324 processed by McCormick et al. (27).

325 For the majority of the study period, we use the PML V2
 326 data set for ET. This data set, when combined with PRISM,
 327 captures subsurface storage deficits consistent with field mea-
 328 surements (27). Since PML V2 is not yet available through
 329 the 2021 water year, we extended the PML V2 data set using
 330 MODIS ET. We bias-corrected MODIS ET to PML V2 using
 331 a basin-specific linear relationship for each study watershed.
 332 For most watersheds, the correlation between PML V2 and
 333 MODIS ET is strong (median $R^2 > 0.4$, see Supplementary
 334 Code (66)).

335 Snowmelt rate was calculated from daily SNODAS data as
 336 in Barnhart et al. (10):

$$337 \quad m = \frac{\sum |\min(\Delta SWE_t, 0)|}{\sum \Delta_t}, \quad [3]$$

338 where the numerator is the sum of all daily differences in SWE
 339 on days when SWE decreases, and Δ_t is 1 on days when SWE
 340 decreases and otherwise 0.

341 The root-zone storage deficit was calculated following Wang-
 342 Erlandsson et al. (36) and Dralle et al. (37). The only dif-
 343 ference here is that instead of using only precipitation and
 344 evapotranspiration (36) or approximating information about
 345 snow using snow cover (37), we used SNODAS data directly
 346 to represent accumulation and melt of snowpack. For a full de-
 347 scription of deficit calculations, see Supplemental Information
 348 S3.

349 **ACKNOWLEDGMENTS.** We would like to thank Sean de Guzman,
 350 chief of the California Department of Water Resources Snow Surveys
 351 and Water Supply Forecasting Section, for providing insight into
 352 how runoff is forecast in California. Funding was provided by Simon
 353 Fraser University, a Natural Sciences and Engineering Research
 354 Council of Canada Discovery Grant, and the USDA Forest Service
 355 Pacific Southwest Research Station with funds administered by Oak
 356 Ridge Institute for Science and Education (ORISE).

357 Open research

358 Data and code generated for this publication are available in an on-
 359 line data repository (66, https://github.com/lapidesd/CA_missing_freshet,
 360). Raster maps of percentiles of April 1 SWE are available at <https://www.hydroshare.org/resource/4b940b8593a4416e954a47bbbc58c568/>
 361 (67). Primary analyses are available as Google Colab notebooks:
 362 (i) exploration of relationship between April 1 SWE and spring
 363 runoff at each study site (<https://colab.research.google.com/drive/1tv8kble9EY3vFdAQzbtIE7RmDpM9uQG?usp=sharing>), (ii) calcula-
 364 tion of all quantities used in analysis and exploring the four hypothe-
 365 ses stated at the end of the introduction (https://colab.research.google.com/drive/1hq-qqllR_LuEyZ5s5RPddnqDLBo4M309?usp=sharing),
 366 (iii) development of a random forest model and a mul-
 367 tiple linear regression model for spring streamflow and
 368 examines the results (<https://colab.research.google.com/drive/1jPtdeESsGPiB2H6MC-W7metpIFsqe799?usp=sharing>), (iv) implemen-
 369 tation of the model described in Section (<https://colab.research.google.com/drive/197Hglpe3kkThdblSFz-9U9h63lvdQzE9?usp=sharing>), and (v)
 370 exploring predictive improvement by adding the deficit at 6 econom-
 371 ically import watersheds in California (https://colab.research.google.com/drive/1_igz4g_mbTntAkPZv3SJGwnYIRUEEBFE?usp=sharing).

378 1. National Operational Hydrologic Remote Sensing Center. Snow data assimilation system
 379 (snodas) data products at nsidc, version 1, 2000.
 380 2. Walter W Immerzeel, AF Lutz, M Andrade, A Bahl, H Biemans, Tobias Bolch, S Hyde, S Brumby,
 381 BJ Davies, AC Elmore, et al. Importance and vulnerability of the world's water towers. *Nature*,
 382 577(7790):364–369, 2020.
 383 3. David R DeWalle and Albert Rango. *Principles of snow hydrology*. Cambridge University
 384 Press, 2008.
 385 4. California Department of Water Resources. Dwr bulletin-120 forecast performance,
 386 water year 2021, 2021. accessed at https://tableau.cnra.ca.gov/t/DWR_Snow_WSFcast/views/WY2021Performance/Dashboard1?%3Adisplay_count=n&%3Aembed=y&%3AisGuestRedirectFromVizportal=y&%3Aorigin=viz_share_link&%3AshowAppBanner=false&%3AshowVizHome=n.
 387 388 389
 390 5. Gabrielle Canon. 'truly an emergency': how drought returned to california – and what lies
 391 ahead. *Guardian*, 2021. accessed at <https://www.theguardian.com/us-news/2021/jun/07/california-drought-oregon-west-climate-change>.
 392 393 394
 395 6. Paul Rogers. Where did sierra snow go this spring? not into California rivers and water
 396 supplies. *The Mercury News*, 2021.
 397 398 399
 400 7. Alan F Hamlet, Philip W Mote, Martyn P Clark, and Dennis P Lettenmaier. Twentieth-century
 401 trends in runoff, evapotranspiration, and soil moisture in the western united states. *Journal of*
 402 *Climate*, 20(8):1468–1486, 2007.
 403 404 405
 406 8. Francesco Avanzi, Joseph Rungee, Tessa Maurer, Roger Bales, Qin Ma, Steven Glaser,
 407 and Martha Conklin. Climate elasticity of evapotranspiration shifts the water balance of
 408 mediterranean climates during multi-year droughts. *Hydrology and Earth System Sciences*,
 409 24(9):4317–4337, 2020.
 410 411 412
 413 9. Martin Hoerling and Jon Eischeid. Past peak water in the southwest. *Southwest Hydrology*, 6
 414 (1):18–19, 2007.
 415 416 417
 418 10. Theodore B Barnhart, Noah P Molotch, Ben Livneh, Adrian A Harpold, John F Knowles, and
 419 Dominik Schneider. Snowmelt rate dictates streamflow. *Geophysical Research Letters*, 43
 420 (15):8006–8016, 2016.
 421 422 423
 424 11. Sarah Boon. Snow ablation energy balance in a dead forest stand. *Hydrological Processes:*
 425 *An International Journal*, 23(18):2600–2610, 2009.
 426 427 428
 429 12. Evan Pugh and Eric Small. The impact of pine beetle infestation on snow accumulation and
 430 melt in the headwaters of the colorado river. *Ecology*, 5(4):467–477, 2012.
 431 432 433
 434 13. Dennis H Knight, Joseph B Yavitt, and Gregory D Joyce. Water and nitrogen outflow from
 435 lodgepole pine forest after two levels of tree mortality. *Forest Ecology and Management*, 46
 436 (3-4):215–225, 1991.
 437 438 439
 440 14. TW Hawkins and AW Ellis. The dependence of streamflow on antecedent subsurface moisture
 441 in an arid climate. *Journal of arid environments*, 74(1):75–86, 2010.
 442 443 444
 445 15. Daniele Penna, HJ Tromp-van Meerveld, Alberto Gobbi, Marco Borga, and Giancarlo
 446 Dalla Fontana. The influence of soil moisture on threshold runoff generation processes in
 447 an alpine headwater catchment. *Hydrology and Earth System Sciences*, 15(3):689–702,
 448 2011.
 449 450 451
 452 16. Daniele Penna, HILDA JACOBA van Meerveld, Omar Oliviero, Giulia Zuecco, RS Assendelft,
 453 Giancarlo Dalla Fontana, and MARCO Borga. Seasonal changes in runoff generation in a
 454 small forested mountain catchment. *Hydrological Processes*, 29(8):2027–2042, 2015.
 455 456 457
 458 17. Jeffrey J McDonnell, Christopher Spence, Daniel J Karan, HJ Ilja van Meerveld, and Ciaran
 459 Harman. Fill-and-spill: A process description of runoff generation at the scale of the beholder.
 460 *Water Resources Research*, page e2020WR027514, 2021.
 461 462 463
 464 18. Takahiro Sayama, Jeffrey J McDonnell, Amod Dhakal, and Kate Sullivan. How much water
 465 can a watershed store? *Hydrological Processes*, 25(25):3899–3908, 2011.
 466 467 468
 469 19. Rodney J Arkley. Soil moisture use by mixed conifer forest in a summer-dry climate. *Soil*
 470 *Science Society of America Journal*, 45(2):423–427, 1981.
 471 472 473
 474 20. Roger C Bales, Jan W Hopmans, Anthony T O'Geen, Matthew Meadows, Peter C Hartsough,
 475 Peter Kirchner, Carolyn T Hunsaker, and Dylan Beaudette. Soil moisture response to snowmelt
 476 and rainfall in a sierra nevada mixed-conifer forest. *Vadose Zone Journal*, 10(3):786–799,
 477 2011.
 478 479 480
 481 21. MA Anderson, RC Graham, GJ Alyanakian, and DZ Martynn. Late summer water status of
 482 soils and weathered bedrock in a giant sequoia grove. *Soil Science*, 160(6):415–422, 1995.
 483 484 485
 486 22. DP Jones and RC Graham. Water-holding characteristics of weathered granitic rock in
 487 chaparral and forest ecosystems. *Soil Science Society of America Journal*, 57(1):256–261,
 488 1993.
 489 490 491
 492 23. DC Lewis and Robert H Burgy. The relationship between oak tree roots and groundwater
 493 in fractured rock as determined by tritium tracing. *Journal of Geophysical Research*, 69(12):
 494 2579–2588, 1964.
 495 496 497
 498 24. Gretchen R Miller, Xingyuan Chen, Yoram Rubin, Siyan Ma, and Dennis D Baldocchi. Ground-
 499 water uptake by woody vegetation in a semiarid oak savanna. *Water Resources Research*, 46
 500 (10), 2010.
 501 502 503
 504 25. K Rose, R Graham, and D Parker. Water source utilization by pinus jeffreyi and arctostaphylos
 505 patula on thin soils over bedrock. *Oecologia*, 134(1):46–54, 2003.
 506 507 508
 509 26. Daniella M Rempe and William E Dietrich. Direct observations of rock moisture, a hidden
 510 component of the hydrologic cycle. *Proceedings of the National Academy of Sciences*, 115
 511 (11):2664–2669, 2018.
 512 513 514
 515 27. Erica L McCormick, David N Dralle, W Jesse Hahm, Alison K Tune, Logan M Schmidt, K Dana
 516 Chadwick, and Daniella M Rempe. Widespread woody plant use of water stored in bedrock.
 517 *Nature*, 597(7875):225–229, 2021.
 518 519 520
 521 28. Michael L Goulden and Roger C Bales. California forest die-off linked to multi-year deep soil
 522 drying in 2012–2015 drought. *Nature Geoscience*, 12(8):632–637, 2019.
 523 524 525
 526 29. P Zion Klos, Michael L Goulden, Clifford S Riebe, Christina L Tague, A Toby O'Geen, Brady A
 527 Flinchum, Mohammad Safeeq, Martha H Conklin, Stephen C Hart, Asmeret Asefaw Berhe,
 528 et al. Subsurface plant-accessible water in mountain ecosystems with a mediterranean climate.
 529 *Wiley Interdisciplinary Reviews: Water*, 5(3):e1277, 2018.
 530 531 532
 533 30. W Jesse Hahm, DM Rempe, DN Dralle, TE Dawson, and WE Dietrich. Oak transpiration
 534 drawn from the weathered bedrock vadose zone in the summer dry season. *Water Resources*
 535 *Research*. 56 (11): e2020WR027419, 56(11), 2020.
 536 537 538

- 462 31. Keirnan JA Fowler, Gemma Coxon, Jim E Freer, Wouter JM Knoben, Murray C Peel, Thorsten
463 Wagener, Andrew W Western, Ross A Woods, and Lu Zhang. Towards more realistic runoff
464 projections by removing limits on simulated soil moisture deficit. *Journal of Hydrology*, 600:
465 126505, 2021.
- 466 32. Kazuhito Ichii, Weile Wang, Hirofumi Hashimoto, Feihua Yang, Petr Votava, Andrew R
467 Michaelis, and Ramakrishna R Nemani. Refinement of rooting depths using satellite-based
468 evapotranspiration seasonality for ecosystem modeling in california. *Agricultural and Forest
469 Meteorology*, 149(11):1907–1918, 2009.
- 470 33. Dara Entekhabi, Eni G Njoku, Peggy E O'Neill, Kent H Kellogg, Wade T Crow, Wendy N
471 Edelstein, Jared K Entin, Shawn D Goodman, Thomas J Jackson, Joel Johnson, et al. The
472 soil moisture active passive (smap) mission. *Proceedings of the IEEE*, 98(5):704–716, 2010.
- 473 34. Felix W Landerer and SC Swenson. Accuracy of scaled grace terrestrial water storage
474 estimates. *Water resources research*, 48(4), 2012.
- 475 35. Keirnan Fowler, Wouter Knoben, Murray Peel, Tim Peterson, Dongryeol Ryu, Margarita
476 Salt, Ki-Weon Seo, and Andrew Western. Many commonly used rainfall-runoff models lack
477 long, slow dynamics: Implications for runoff projections. *Water Resources Research*, 56(5):
478 e2019WR025286, 2020.
- 479 36. Lan Wang-Erlandsson, Wim GM Bastiaanssen, Hongkai Gao, Jonas Jägermeyr, Gabriel B
480 Senay, Albert IJM Van Dijk, Juan P Guerschman, Patrick W Keys, Line J Gordon, and
481 Hubert HG Savenije. Global root zone storage capacity from satellite-based evaporation.
482 *Hydrology and Earth System Sciences*, 20(4):1459–1481, 2016.
- 483 37. David N Dralle, W Jesse Hahm, K Dana Chadwick, Erica McCormick, and Daniella M Rempe.
484 Accounting for snow in the estimation of root zone water storage capacity from precipitation
485 and evapotranspiration fluxes. *Hydrology and Earth System Sciences*, 25(5):2861–2867,
486 2021.
- 487 38. James W Roche, Qin Ma, Joseph Rungee, and Roger C Bales. Evapotranspiration mapping
488 for forest management in california's sierra nevada. *Frontiers in Forests and Global Change*,
489 3:69, 2020.
- 490 39. J Grindley. Calculated soil moisture deficits in the dry summer of 1959 and forecast dates of
491 first appreciable runoff. *Int. Ass. Sci. Hydrol.*, pages 109–20, 1960.
- 492 40. Alys C Thomas, John T Reager, James S Famiglietti, and Matthew Rodell. A grace-based
493 water storage deficit approach for hydrological drought characterization. *Geophysical Research
494 Letters*, 41(5):1537–1545, 2014.
- 495 41. A Geruo, Isabella Velicogna, John S Kimball, Jinyang Du, Youngwook Kim, Andreas Colliander,
496 and Eni Njoku. Satellite-observed changes in vegetation sensitivities to surface soil moisture
497 and total water storage variations since the 2011 texas drought. *Environmental Research
498 Letters*, 12(5):054006, 2017.
- 499 42. Lauren Lowman and Ana Paula Barros. Fire-induced canopy changes alter plant water, energy
500 and carbon relations for coastal plains forests in the southeast us. In *AGU Fall Meeting
501 Abstracts*, volume 2019, pages B53H–2500, 2019.
- 502 43. Gabrielle Boisramé, Sally Thompson, Brandon Collins, and Scott Stephens. Managed wildfire
503 effects on forest resilience and water in the sierra nevada. *Ecosystems*, 20(4):717–732, 2017.
- 504 44. Juli G Pausas and Jon E Keeley. Wildfires as an ecosystem service. *Frontiers in Ecology and
505 the Environment*, 17(5):289–295, 2019.
- 506 45. Heidi J Renninger, Kenneth L Clark, Nicholas Skowronski, and Karina VR Schäfer. Effects
507 of a prescribed fire on water use and photosynthetic capacity of pitch pines. *Trees*, 27(4):
508 1115–1127, 2013.
- 509 46. Geeta G Persad, Daniel L Swain, Claire Kouba, and J Pablo Ortiz-Partida. Inter-model agree-
510 ment on projected shifts in california hydroclimate characteristics critical to water management.
511 *Climatic Change*, 162(3):1493–1513, 2020.
- 512 47. VM Castillo, A Gomez-Plaza, and M Martinez-Mena. The role of antecedent soil water content
513 in the runoff response of semiarid catchments: a simulation approach. *Journal of Hydrology*,
514 284(1-4):114–130, 2003.
- 515 48. Thomas Dunne and Richard D Black. An experimental investigation of runoff production in
516 permeable soils. *Water Resources Research*, 6(2):478–490, 1970.
- 517 49. R Allan Freeze. Role of subsurface flow in generating surface runoff: 1. base flow contributions
518 to channel flow. *Water Resources Research*, 8(3):609–623, 1972.
- 519 50. W Jesse Hahm, DN Dralle, DM Rempe, AB Bryk, SE Thompson, TE Dawson, and WE Dietrich.
520 Low subsurface water storage capacity relative to annual rainfall decouples mediterranean
521 plant productivity and water use from rainfall variability. *Geophysical Research Letters*, 46(12):
522 6544–6553, 2019.
- 523 51. W Steven Holbrook, Clifford S Riebe, Mehrez Elwaseif, Jorden L. Hayes, Kyle Basler-Reeder,
524 Dennis L. Harry, Armen Malazian, Anthony Dosseto, Peter C. Hartsough, and Jan W. Hopmans.
525 Geophysical constraints on deep weathering and water storage potential in the southern sierra
526 critical zone observatory. *Earth Surface Processes and Landforms*, 39(3):366–380, 2014.
- 527 52. Jonathan A Wald, Robert C Graham, and Phillip J Schoeneberger. Distribution and properties
528 of soft weathered bedrock at ≤ 1 m depth in the contiguous united states. *Earth Surface
529 Processes and Landforms*, 38(6):614–626, 2013.
- 530 53. Ronald Amundson, Arjun Heimsath, Justine Owen, Kyungsoo Yoo, and William E Dietrich.
531 Hillslope soils and vegetation. *Geomorphology*, 234:122–132, 2015.
- 532 54. U.S. Geological Survey. National water information system data available on the world wide
533 web (water data for the nation), 2021. accessed December 2021.
- 534 55. PRISM Climate Group. Prism rainfall dataset, 2004. accessed at <http://prism.oregonstate.edu>.
- 535 56. Yongqiang Zhang, Dongdong Kong, Rong Gan, Francis HS Chiew, Tim R McVicar, Qiang
536 Zhang, and Yuting Yang. Coupled estimation of 500 m and 8-day resolution global evapotran-
537 spiration and gross primary production in 2002–2017. *Remote Sensing of Environment*, 222:
538 165–182, 2019.
- 539 57. Rong Gan, Yongqiang Zhang, Hao Shi, Yuting Yang, Derek Eamus, Lei Cheng, Francis HS
540 Chiew, and Qiang Yu. Use of satellite leaf area index estimating evapotranspiration and gross
541 assimilation for australian ecosystems. *Ecohydrology*, 11(5):e1974, 2018.
- 542 58. Yongqiang Zhang, Jorge L Peña-Arancibia, Tim R McVicar, Francis HS Chiew, Jai Vaze,
543 Changming Liu, Xingjie Lu, Hongxing Zheng, Yingping Wang, Yi Y Liu, et al. Multi-decadal
544 trends in global terrestrial evapotranspiration and its components. *Scientific reports*, 6(1):1–12,
545 2016.
59. S. Running, Q. Mu, and M. Zhao. Mod16a2 modis/terra net evapotranspiration 8-day I4 global
546 500m sin grid v006 [data set]. nasa eosdis land processes daac, 2017.
60. Noel Gorelick, Matt Hancher, Mike Dixon, Simon Ilyushchenko, David Thau, and Rebecca
548 Moore. Google earth engine: Planetary-scale geospatial analysis for everyone. *Remote
549 sensing of Environment*, 202:18–27, 2017.
61. MC Anderson, JM Norman, GR Diak, WP Kustas, and JR Mecikalski. A two-source time-
551 integrated model for estimating surface fluxes using thermal infrared remote sensing. *Remote
552 sensing of environment*, 60(2):195–216, 1997.
62. Martha C Anderson, John M Norman, John R Mecikalski, Jason A Otkin, and William P
554 Kustas. A climatological study of evapotranspiration and moisture stress across the continental
555 united states based on thermal remote sensing: 1. model formulation. *Journal of Geophysical
556 Research: Atmospheres*, 112(D10), 2007.
63. Martha C Anderson, John M Norman, John R Mecikalski, Jason A Otkin, and William P
558 Kustas. A climatological study of evapotranspiration and moisture stress across the continental
559 united states based on thermal remote sensing: 2. surface moisture climatology. *Journal of
560 Geophysical Research: Atmospheres*, 112(D11), 2007.
64. Martha C Anderson, Christopher Hain, Brian Wardlow, Agustin Pimstein, John R Mecikalski,
562 and William P Kustas. Evaluation of drought indices based on thermal remote sensing of
563 evapotranspiration over the continental united states. *Journal of Climate*, 24(8):2025–2044,
564 2011.
65. Soil Survey Staff. Gridded national soil survey geographic (gnatsgo) database for the con-
566 tinuous united states, 2019. <https://nrsc.app.box.com/v/soils>.
66. Dana A Lapidés, W Jesse Hahm, Daniella M Rempe, and David N Dralle. Supplementary
568 code and data for: Root zone storage deficits mediate the production of streamflow from
569 snowmelt, 2021. accessed at https://github.com/lapidesd/CA_missing_freshet.
67. Dana A Lapidés, W Jesse Hahm, Daniella M Rempe, and David N Dralle. April 1 swe spatial
571 percentiles using snodas for the contiguous usa, 2021. accessed at <https://www.hydroshare.org/resource/4b940b8593a4416e954a47bbbc58c56b/>.

1

2 **Supplementary Information for**

3 **Missing snowmelt runoff following drought explained by root-zone storage deficits**

4 **Dana A Lapidés, W Jesse Hahm, Daniella M Rempe, David N Dralle**

5 **Dana A Lapidés.**

6 **E-mail: dlapides@sfu.ca**

7 **This PDF file includes:**

8 Supplementary text

9 Figs. S1 to S5

10 Tables S1 to S4

11 SI References

12 **Supporting Information Text**

13 **Site description and site selection**

14 California experiences a Mediterranean climate with cool, wet winters and hot, dry summers. In much of California, wet season
 15 precipitation arrives as rain, but mountainous regions such as the Sierra Nevada predominantly receive snow. Mediterranean
 16 regions generally have highly variable annual precipitation (1) and are subject to rapid switches between drought and flood
 17 conditions (2, 3). California has a particularly variable climate due to the added influence of complex topography (4). In the
 18 past decade, California has experienced extreme drought (5–7) that resulted in extensive wildfires (8, 9) and tree mortality
 19 (10–12), and periods of extraordinarily high precipitation (13, e.g., winter 2016-2017;) that resulted in widespread flooding (13)
 20 and landslides (14).

Site	Stream name	Gage location	Area [km ²]	MAP [mm]	Snow percent	Mean Annual Q [mm]
Pristine basins:						
10336780	Trout Creek	-119.972, 38.9199	95	893	67	315
10336645	General Creek	-120.118, 39.0518	19	1202	58	740
10336660	Blackwood Creek	-120.162, 39.1074	29	1486	59	1018
10336676	Ward Creek	-120.157, 39.1321	25	1549	61	885
10343500	Sagehen Creek	-120.237, 39.4315	27	976	65	319
10308783	Leviathan Creek	-119.656, 38.7012	11	635	60	50
11383500	Deer Creek	-121.948, 40.0140	539	1484	32	499
11189500	SF Kern River	-118.173, 35.7374	1373	477	36	72
11204100	SF Tule River near Reservation	-118.813, 36.0241	248	798	25	128
11203580	SF Tule River near Cholollo Camp	-118.654, 36.0482	52	996	44	278
11266500	Merced River at Pohono Bridge	-119.666, 37.7168	831	1213	60	685
11264500	Merced River at Happy Isles Bridge	-119.558, 37.7315	469	1199	68	673
10265150	Hot Creek	-118.817, 37.6688	177	814	72	262
Basins essential for California water supply:						
11525500	Trinity River	-122.804, 40.7193	1862	1445	17	405
11377100	Sacramento River	-122.187, 40.2885	23051	972	27	426
11270900	Merced River	-120.332, 37.5216	2748	1032	29	399
11289650	Tuolumne River	-120.442, 37.6663	3983	1098	37	222
11319500	Mokelumne River below Merced Falls	-120.720, 38.3127	1408	1265	38	612
11335000	Cosumnes River	-121.045, 38.5002	1388	1073	13	292

Table S1. Catchment attributes for study sites. Streamflow and basic site information are from NWIS (15), and climate information are derived from GAGES-II (16).

21 To explore drivers of low streamflow in 2021 in California, we examined a set of minimally disturbed, gauged watersheds in
 22 the Sierra Nevada (Figure 1c in main text). Sites were selected in the Sierra Nevada that met the following criteria:

- 23 1. no upstream dams (16),
- 24 2. >20% precipitation falls as snow annually on average (16),
- 25 3. watershed boundaries were delineated in NHD+ (17),
- 26 4. <5% developed land cover (18),
- 27 5. <5% cultivated land cover (18),
- 28 6. <35% burned area between 1990 and 2020 (19),
- 29 7. <20% logged area (20),
- 30 8. at least 10 years with continuous streamflow from April 1 - September 1 (15),
- 31 9. streamflow record includes 2021 (15).

32 All gages that met these criteria were reviewed manually to ensure hydrographs appear unmodified and snowmelt-dominated.
 33 We identified 13 catchments that met the selection criteria (Table S1), spread throughout the Sierra Nevada. The sites
 34 encompass a range in size from 11 to 1,373 km², annual precipitation from 369 to 979 mm, and a mean streamflow from 0.3 to
 35 190 m³/s. About half of the sites drain to the west, while the remaining sites (primarily those in the Tahoe area) drain to
 36 the east. Additionally, six basins essential to California's water supply were also included to demonstrate applicability of the
 37 presented methods to larger and more complex basins (bottom of Table S1).

38 Model description

39 Hahm et al. (21) developed a stochastic hydrological model incorporating root zone storage as a simple 1-d bucket that
 40 describes annual runoff dynamics in Mediterranean catchments. Similar to Figure 2 in the main text, the model describes
 41 a landscape with thin soil but a substantial weathered bedrock zone that stores plant-accessible water. The entire soil and
 42 weathered bedrock zone is treated as a single plant-accessible storage reservoir S [L]. During the wet season, precipitation P
 43 [L] contributes water to storage, and evapotranspiration ET [L] removes water from storage primarily during the dry season.
 44 Streamflow is generated only if the subsurface storage reservoir is full.

45 Hahm et al. (21), however, did not consider the scenario in which deficits were not replenished and could carry over between
 46 years. Evidence from field observations of soil and rock moisture and tree mortality (22, 23) and from water balance approaches
 47 using satellite data products (24–26) shows that root zone storage deficits can grow over multiple years, meaning that the
 48 deficit can vary substantially between years in a way that is important for vegetation response. Fowler et al. (27) also recently
 49 found that many hydrological models that lack the ability to generate multi-year deficits are unable to simulate streamflow
 50 conditions through multi-year droughts in Australia. Changes in subsurface storage (and deficit) give watersheds “memory”
 51 of prior precipitation that can persist. Peterson et al. (28) found that more than 8 years after the Millennium Drought in
 52 southeastern Australia, many watersheds had not returned to pre-drought conditions. They inferred that enhanced evaporation
 53 due to warmer conditions slowed recharge to the subsurface so that deficits generated during the Millennium Drought still
 54 were not satisfied. Thus, changes in ET can impact streamflow generation and also provide a feedback that strengthens the
 55 importance of subsurface storage deficit on streamflow.

56 Here, we extend the model presented by Hahm et al. (21) to allow for both multi-year deficit accrual and snow. To allow for
 57 multi-year deficit accrual, we explicitly track a timeseries of annual October 1 deficit so that initial water year conditions may
 58 vary between years, and to account for snow, we add a snowmelt period following the wet season (during which rain enters
 59 storage and snow accumulates), with the April 1 snowpack SWE [L] delivered at a rate of m [L/T]. Hahm et al. (21) assumed
 60 that cumulative wet season ET is constant from year to year, an assumption that was meant to reflect the fact that ET is
 61 energy-limited during the cold wet season in California. When considering the snowmelt period, though, ET total may not be
 62 constant between years since the length of the snowmelt period can vary substantially depending on the snowmelt rate m [L/T]
 63 and the size of the snowpack SWE . This dynamic can be accounted for in the snowmelt period by considering ET during the
 64 melt period and post-snowmelt growing period as energy-determined rates ET_s [L/T] and ET_{summer} [L/T] that last for the
 65 duration of the melt period and summer respectively. Then, the total warm season $ET_{warm} = N_{melt}ET_s + N_{warm_dry}ET_{summer}$
 66 [L], where N_{melt} [T] and N_{warm_dry} [T] are the lengths of the melt period and post-snowmelt growing season, respectively.

Thus, the extended model includes three seasons with distinct fluxes: a winter wet season, a snowmelt period, and a
 snowmelt-free growing season:

$$S_{Apr1} = \min(S_{max}, \max(0, S_{Oct1} + P_w - ET_w)), \quad [1]$$

$$S_{Aug1} = \min(S_{max}, \max(0, S_{Apr1} + SWE - (ET_s - P_s)N_{melt})), \quad [2]$$

$$S_{Oct1} = \max(0, S_{Aug1} - ET_{summer}N_{warm_dry}), \quad [3]$$

67 where S_{Apr1} [L] is the root zone storage at the start of the snowmelt period, S_{Aug1} [L] is the root zone storage at the start of
 68 the post-snowmelt growing period, and S_{Oct1} [L] is the root zone storage at the start of the winter wet season. S_{max} [L] is the
 69 maximum possible value of root-zone storage, ET_w [L] is winter ET, and P_w [L] and P_s [L/T] are winter and spring rainfall.
 70 Because storage is constrained between 0 and S_{max} , ET cannot occur if storage is empty, and runoff is generated if storage
 71 is full, which can happen during the winter wet season or during the snowmelt period. Equation 1 describes the winter wet
 72 season when rain increases storage and ET draws from storage, Equation 2 the melt period when SWE melts into storage and
 73 a net ET flux draws from storage, and Equation 3 the post-melt growing season when ET draws from storage. For simplicity,
 74 we define a single term $ET_{net} = ET_s - P_s$ that describes the potential net ET during the melt period, and ET_{summer} can be
 75 considered in the same way in regions with significant precipitation during the growing season.

76 By using the mass balance from Equations 1-3, streamflow during the snowmelt period is given by:

$$Q = \begin{cases} \max(0, SWE - ET_{net}N_{melt}), & \text{if } P_w - ET_w > D_{Oct1} \\ \max(0, SWE - ET_{net}N_{melt} - D_{Oct1} + (P_w - ET_w)), & \text{otherwise} \end{cases} \quad [4]$$

78 where Q [L] is total streamflow due to snowmelt, and D_{Oct1} [L] is the root zone storage deficit ($S_{max} - S_{Oct1}$) at the end of
 79 the preceding dry season. Both conditions are bounded by 0 since streamflow cannot be negative. A negative value for either
 80 condition indicates that water demand from ET exceeds water availability from rain, snowmelt, and storage, so streamflow
 81 must be 0.

82 In Equation 4, there are three terms that can cause the relationship between SWE and Q to be non-unique: (i) the total net
 83 ET flux during the melt period ($(ET_s - P_s)N_{melt}$), which is impacted indirectly by the melt rate m since $m = SWE/N_{melt}$,
 84 (ii) the root zone storage deficit at the end of the dry season D_{Oct1} (referred to as Oct. 1 deficit), which is driven by ET,
 85 precipitation, and runoff dynamics during prior years, and (iii) winter recharge ($P_w - ET_w$). Increasing total ET during the
 86 snowmelt period ($ET_{net}N_{melt}$) reduces streamflow generation. This ET term can be increased by increasing vegetation demand
 87 (increased ET_{net}), reducing spring rainfall (increased ET_{net}), or by slowing down the snowmelt rate m (increased length of
 88 N_{melt} for the same SWE). While increasing the October 1 deficit reduces streamflow generation, increasing winter recharge
 89 ($P_w - ET_w$) can increase streamflow generation. This can be achieved either by increasing P_w (decreasing annual snow fraction

90 since SWE remains constant) or decreasing ET_w (reducing winter ET), so long as storage is not already being filled up. See
 91 Supplemental Information S2 for a visual demonstration of how each parameter impacts Q . Any of these mechanisms could
 92 confound a linear regression model for streamflow based only on April 1 SWE.

93 Subsurface deficit calculations

94 To estimate a storage deficit in the subsurface (D), we adapted the method presented by Wang-Erlandsson et al. (25) and
 95 updated to account for snow cover by Dralle et al. (29). In this method, root zone storage deficit is calculated as the running
 96 difference between fluxes leaving (F_{out} [L/T]) and entering (F_{in} [L/T]) the system during a time interval defined by the
 97 sampling frequency of remotely sensed products. Generally, F_{out} is set equal to ET , neglecting streamflow, and F_{in} is set equal
 98 to precipitation. Dralle et al. (29) used snow cover data from satellite products to adjust fluxes in snow-dominated regions.
 99 Here, since we have access to explicit information on snow through SNODAS (30), we incorporate snow directly into the mass
 100 balance approach by defining F_{in} as

$$101 \quad F_{in} = P_r + Q_m, \quad [5]$$

102 where P_r is precipitation falling as rain determined as precipitation when SWE does not increase, and Q_m is given by decreases
 103 in SWE. More precisely,

$$104 \quad P_{r,t_n} = P_{t_n} - \max(\text{SWE}_{t_n} - \text{SWE}_{t_{n-1}}, 0), \quad [6]$$

105 where P_i is the total precipitation falling in timestep i and SWE_i is the SWE at time step i and

$$106 \quad Q_m = \max(\text{SWE}_{t_{n-1}} - \text{SWE}_{t_n}, 0). \quad [7]$$

107 Following the deficit tracking procedure presented by Wang-Erlandsson et al. (25), we proceed by calculating the difference
 108 between F_{out} and F_{in} over a time interval from t_n to t_{n+1} :

$$109 \quad A_{t_n \rightarrow t_{n+1}} = \int_{t_n}^{t_{n+1}} (F_{out} - F_{in}) dt. \quad [8]$$

110 This accumulated difference ($A_{t_n \rightarrow t_{n+1}}$) is a *deficit*, so the signs of fluxes are reversed compared to a traditional mass balance.
 111 If the accumulated difference is negative, then no deficit has been accrued in the time step. So, a lower bound on root zone
 112 storage deficit for each time step is given by the maximum value of zero and the running sum of accumulated differences:

$$113 \quad D(t_{n+1}) = \max(0, D(t_n) + A_{t_n \rightarrow t_{n+1}}) \quad [9]$$

114 **Runoff is not needed to calculate accurate deficits.** For a couple of reasons, it is neither appropriate nor necessary to account
 115 for runoff in root-zone storage deficit calculations. First, water drainage from the root zone during precipitation or snowmelt
 116 can sustain streamflow production for weeks, even months, following the drainage event. This temporal mismatch between
 117 root-zone drainage and flow generation in the stream implies that any deficit generation related to flow production likely
 118 occurred well before the observation of flow; therefore, using streamflow in deficit calculations would increase deficits at the
 119 wrong time. One approach for accounting for runoff in deficit calculations might be to incorporate a root-zone drainage term,
 120 which is not straightforward to measure or estimate. However, this is not necessary as the drainage flux should have a minimal
 121 impact on deficit growth; significant drainage occurs primarily when the deficit is small or zero due to water inputs (snowmelt
 122 or precipitation), and this root-zone drainage flux is likely smaller than the water fluxes that generate drainage (as is accepted
 123 in modeling studies and suggested by findings of runoff ratios smaller than 1 in empirical studies; 31–33), meaning that the net
 124 change to the deficit would be negligible. Since the deficit is small or zero when drainage occurs, and inputs likely exceed
 125 the drainage flux, true deficit growth is unlikely to occur during drainage events. As a result, neglecting drainage in deficit
 126 calculations should not have a significant impact on calculated root-zone storage deficits.

127 Factors that impact spring streamflow generation

Panel	S_{max}	ET_{warm}	ET_w	μ	sd	snowfrac	m
a	1,000	10-300	0	400	100	1	10
b	300	800	0	700	150	0.7	10-50
c	1,000	350	0	400	100	1	10
d	300	300	0	400	100	0.25-1	10

Table S2. Parameter values used to generated each subfigure in Figure S1: S_{max} is maximum root zone storage; PET is total potential evapotranspiration in the warm season; ET_w in the winter; μ and sd are parameters for the gamma distribution for annual precipitation; snowfrac is the fraction of annual precipitation that falls as snow; and m is the snowmelt rate.

128 As described in the main text, the relationship between April 1 SWE and spring streamflow is not unique. Within a mass
 129 balance framework, there are four factors that can drive lower spring streamflow: (a) more net spring ET (ET-rain), (b) a slower
 130 snowmelt rate, (c) a larger root zone storage deficit, or (d) less rainfall. Figure S1 uses the mass balance model to show directly
 131 how each of these four factors affects the resulting spring streamflow. For this exercise, we use this total ET_{warm} to set an

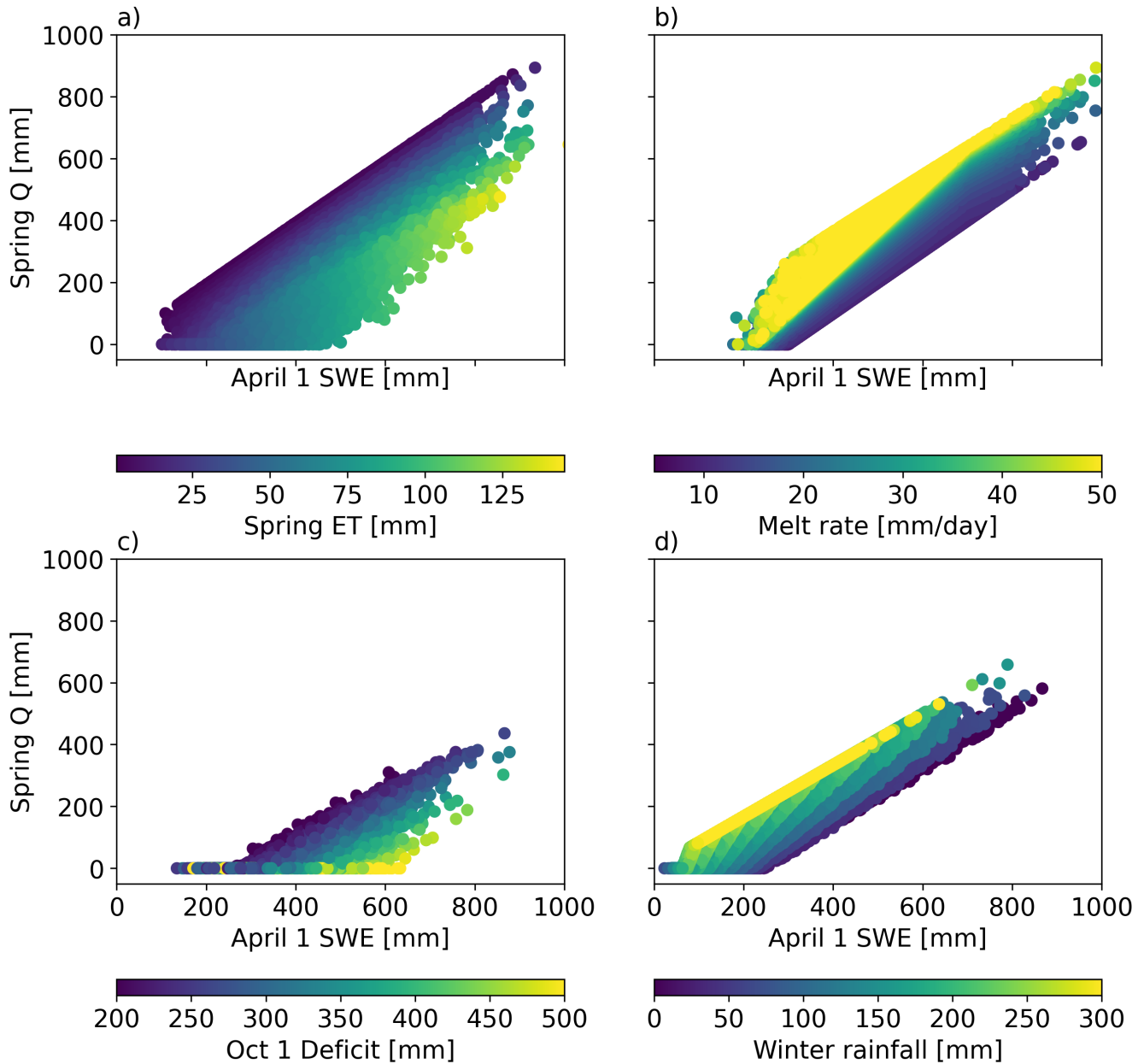


Fig. S1. Differences in (a) spring evapotranspiration (ET), (b) snow melt rate, (c) root zone storage deficit, and (d) winter rainfall can result in different spring streamflow from the same April 1 SWE, as shown by Monte Carlo simulations with annual precipitation P selected from a gamma distribution and April 1 SWE given as a fraction of P . Parameters used to generate this figure are shown in Table S2. Melt rate is calculated assuming a 180 day warm season.

132 average rate of ET during the warm season that is applied to both the snowmelt period and post-snowmelt growing season. We
 133 apply Equations 1-3 to track storage through time. Parameters S_{max} , ET_w , and $ET_{warm} = ET_s N_{melt} + ET_{summer} N_{warm_dry}$
 134 are the same each year, while P_w , P_s , SWE , and the partitioning of ET_{warm} between the snowmelt period and the snow-free
 135 growing season vary between years. A spinup period of 100 years is used to generate initial conditions. For each year, we
 136 select an annual precipitation from a gamma distribution. Since spring rainfall is included in the term ET_{net} , we do not
 137 explicitly include that rainfall in the annual precipitation. Instead, we allow SWE and P_w to add to the gamma-selected
 138 annual precipitation, with the partition described by a fraction ($snowfrac$). This setup still results in a gamma distribution for
 139 annual precipitation since the spring rainfall is constant. Throughout the simulation period, we track storage deficits generated
 140 at the end of each growing season, SWE , and snowmelt runoff calculated for each year using Equation 4. Parameters used to
 141 generate the figure are in Table S2.

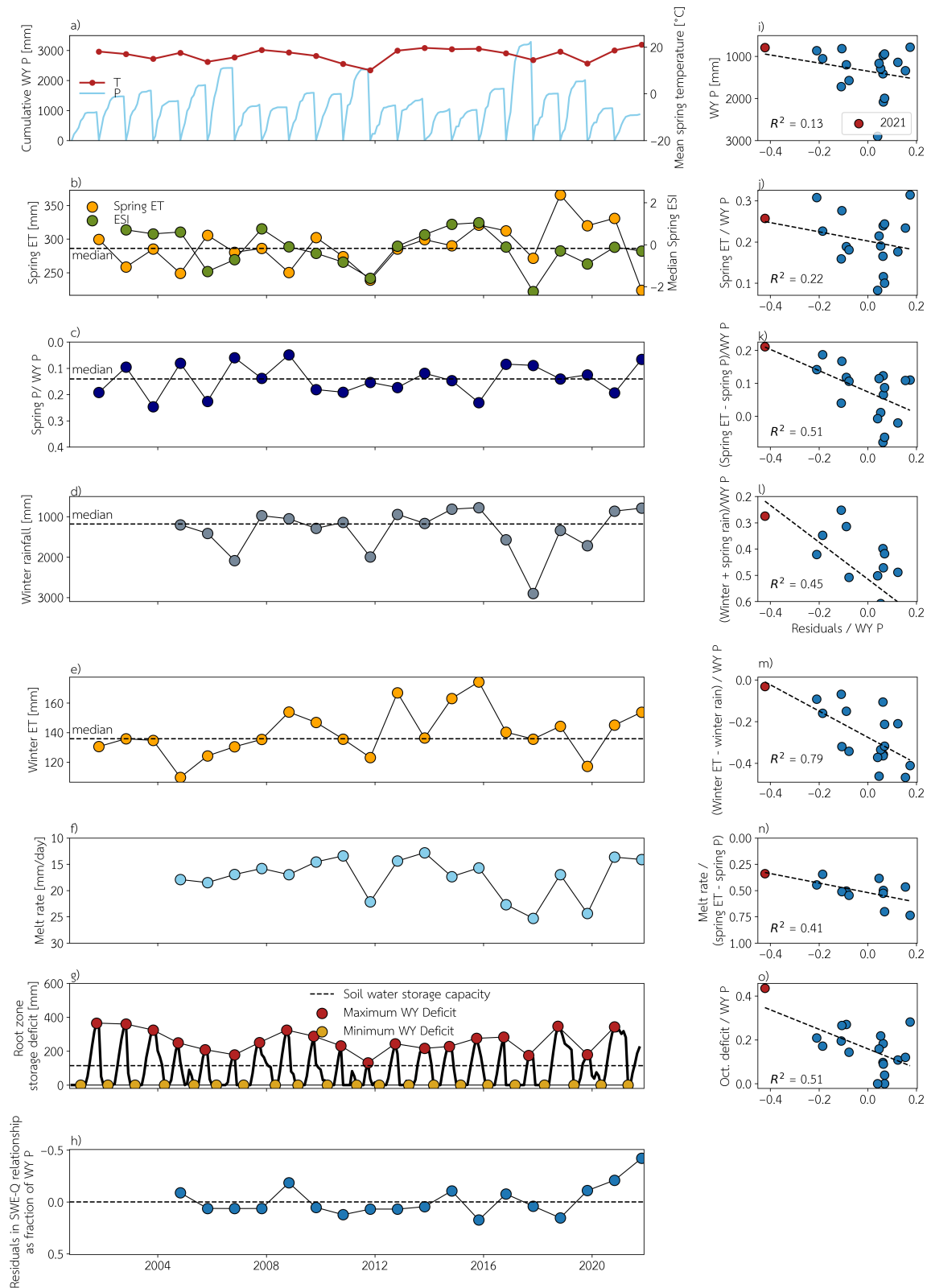


Fig. S2. Water year data for one representative study site (Ward Ck). Spring ET and spring P are for the months April-July. All panels are oriented so that moving vertically in the panel theoretically results in less spring streamflow. In particular, note that the y-axes for panels c, e, h, i, and m and the x-axis for panels g-k are reversed. As a result, all relationships in panels g-k should appear negative. Red scatter points in panels g-k mark the 2021 water year.

142 **Exploratory analysis of variables that impact melt period streamflow**

143 We performed exploratory data analysis to quantify the importance of each variable that appears in Equation 4 for explaining
 144 residuals in snowpack-runoff relationships. This analysis was used to select a minimal set of variables that both encompass

Table S3. Parameters for the multiple linear regression model to predict spring streamflow. For parameter descriptions, see Table 1 in the main text. Parameter values are shown multiplied by median absolute variable values among (top) top 25th percentile wettest years and (below) driest 25th percentile of water years and shown in units of mm for comparison. Values marked by an asterisk indicate that the sign is opposite to the expected sign based on hypothesized mechanisms. Parameter columns are listed in order of decreasing median effect size, so SWE has the largest effect size, and m/ET_{net} the smallest across the study sites.

Site	SWE	$\frac{P_w + P_s}{P}$	$\frac{D_{Oct1}}{P}$	$\frac{ET_{net} N_{melt}}{P}$	$\frac{ET_w - P_w}{P}$	$\frac{m}{ET_{net}}$
Wet years						
10336780	560	63	-15	2*	-0	-1*
10336645	929	61	-18	-2	-6	-10*
10336660	1195	21	-82	-2	-109	9
10336676	1268	144	-72	-5	-50	3
10343500	715	37	-28	0	-41	-78*
10308783	43	18	-19	-29	-5	53
11383500	118	236	-23	-6	-82	-2*
11189500	94	-26*	-0	-9	-9	8
11204100	31	212	-12	-25	12*	1
11203580	83	160	-17	-32	-42	6
11266500	1000	59	-15	-5	-36	22
11264500	927	77	-13	-10	-6	8
10265150	56	6	-3	-2	-12	1
Median	560	61	-17	-5	-12	3
Dry years						
10336780	156	126	-66	4*	-2	-1*
10336645	144	124	-99	-27	-38	-5*
10336660	472	21	-217	-96	-89	6
10336676	573	145	-199	-84	-38	2
10343500	240	73	-92	1	-32	-29*
10308783	2	20	-39	-64	-2	21
11383500	34	215	-63	-57	-57	-1*
11189500	9	-33*	-1	-23	-3	5
11204100	1	210	-49	-87	4*	0
11203580	6	162	-62	-134	-10	2
11266500	197	87	-112	-29	-25	17
11264500	225	118	-87	-18	-2	10
10265150	12	8	-61	-28	-2	1
Median	144	118	-66	-29	-10	2

Table S4. Performance of the multiple linear regression model to predict spring streamflow. For parameter descriptions, see Table 1 in the main text. R^2 values are shown for full model, a model using only April 1 SWE and D_{Oct1} / P_w as variables, and a model only using April 1 SWE. The latter two models can both be run prior to snowmelt. The final two columns compare the R^2 value for a regression model using only April 1 SWE on the years following the top 25th percentile years versus the bottom 25th percentile of years in terms of annual precipitation.

Site	R^2 (all params)	R^2 (SWE, $\frac{D_{Oct1}}{P_w}$)	R^2 (SWE)	R^2 after wet years	R^2 after dry years
10336780	0.94	0.90	0.87	0.91	0.13
10336645	0.93	0.90	0.88	0.59	0.40
10336660	0.96	0.93	0.87	0.65	0.51
10336676	0.98	0.95	0.88	0.75	0.56
10343500	0.98	0.79	0.73	-1.64	0.30
10308783	0.87	0.64	0.63	0.88	-0.21
11383500	0.78	0.58	0.49	-1.93	-1.20
11189500	0.87	0.75	0.83	0.85	-0.75
11204100	0.91	0.72	0.49	-1.28	-25.06
11203580	0.92	0.73	0.64	-0.07	-8.11
11266500	0.96	0.92	0.91	0.60	0.75
11264500	0.93	0.90	0.89	0.38	0.84
10265150	0.81	0.71	0.65	-0.06	-0.23
Median	0.93	0.85	0.83	0.59	0.13

145 all of the proposed mechanisms for failure of the SWE-Q model but minimizes correlation between variables. To do this, we
 146 wanted to select only one variable to represent each proposed mechanism. Exploratory analysis was used to find one variable
 147 for each mechanism that most strongly correlates with residuals in the SWE-Q model.

148 Figure S2h shows the time series of residuals in the April 1 SWE-spring Q relationship (referred to hereafter as the SWE-Q

149 relationship). Across all sites, 2021 generally stands out as the largest negative residual as a fraction of WY P (note reversed
150 y-axis). See the data supplement to review residual timeseries for all study sites (34). This finding indicates that less streamflow
151 arrived than expected, and the missing streamflow was a substantial portion of the water budget. Based on the parsimonious
152 model described in the main text, we explore four hypotheses to explain why 2021 spring streamflow was lower than expected
153 at the 13 study sites. Results are shown in Figure S2 for Ward Creek (site 10336676), but results across the study sites are
154 qualitatively similar (34, see data supplement;). We selected Ward Creek since it has the highest-performing multiple linear
155 regression model but is otherwise representative of the trends and site characteristics across the study sites.

156 **Hypothesis 1: ET was larger than usual.**

157 **Spring net ET was unusually high.** In 2021, spring ET was lower than usual (Figure S2b) despite high spring temperatures (Figure
158 S2a). The Evaporative Stress Index (ESI) data indicate that plants were water-stressed in 2021 (Figure S2b). While ET
159 was not higher than usual, spring ET accounted for a larger fraction of the annual water budget than usual since annual
160 precipitation was very low (Figure S2a). However, spring ET alone does not explain the magnitude of the residual from the
161 SWE-Q relationship in 2021. Spring ET / WY P explains only 22% of variance in the residuals at Ward Creek (Figure S2j),
162 compared to 13% explained just by WY P (Figure S2i). Over all sites, the median R^2 is 22% for Spring ET / WY P.

163 Spring rain accounted for a much smaller fraction of annual precipitation than usual in 2021, about half of the median
164 (Figure S2c). As with spring ET in 2021, though, spring P fraction was not outside the range of previously observed values.

165 Since net spring ET (ET_{net}) is defined as the difference between spring ET and spring rain, the deviations in the individual
166 terms are combined in ET_{net} . Neither spring ET nor spring rain were outside the range observed in prior years, but ET_{net} was
167 unprecedented in 2021 (red scatter point in Figure S2k). ET_{net} both singles out 2021 as a unique year and explains 51% of
168 variance in the residuals at Ward Creek (Figure S2i). Across all sites, the median R^2 value between residuals and ET_{net} is 0.38.

169 **Winter recharge was unusually low.** A primary control on winter recharge is winter rainfall P_w since snow does not recharge until it
170 melts. Winter rainfall in 2021 was lower than usual, among the lowest winter rainfall years in the study period (Figure S2d)
171 but not outside the range of previously observed values. The other factor controlling winter recharge is winter ET. While
172 spring ET was low in the 2021 WY, this was not the case for winter ET, which was higher than normal (Figure S2e). This
173 finding is exaggerated as a fraction of WY P since 2021 was a dry year (Figure S2m). As with ET_{net} , $(ET_w - P_w) / WY P$
174 singles out 2021 as a particularly extreme year with the highest relative ET_w in the study period, an observation that holds for
175 9 of the 13 study sites, and accounts for 79% of variance in the residuals at Ward Creek. Across all study sites the median
176 variance explained is 38%, indicating that winter recharge has a predictive power similar to spring net ET.

177 **Hypothesis 2: Winter and spring total rainfall was lower than usual.** Both winter rainfall and spring rainfall were lower than
178 usual in the 2021 water year. When combining all winter-spring rain (similar to a snow fraction), rain / WY P explains 45% of
179 the variance in the residuals in the SWE-Q relationship at Ward Creek (Figure S2l). Across all sites, the median is 25%.

180 **Hypothesis 3: Melt rate was unusually slow.** By examining Figure S2f, it is clear that the melt rate in 2021 was slower than
181 usual at Ward Creek, among the slowest melt rates observed in the time period 2003-2021, although not outside the previously
182 observed range. A slow melt rate can reduce streamflow by allowing plants to take greater advantage of snowmelt for ET,
183 which means that it is not melt rate alone but its ratio to ET_{net} that drives the impact of melt rate on streamflow generation,
184 since $m = SWE/N_{melt}$ (see Equation 4). In 2021, the ratio m/ET_{net} was the smallest observed during the study period, and it
185 explains 41% of the variance in the residuals at Ward Creek (Figure S2n). At all other study sites, though, m/ET_{net} generally
186 explains less than 20% of variance or even less than 5% for most sites, with a median of 6%.

187 **Hypothesis 4: Root zone storage deficit was unusually large.** Each year, the root zone storage deficit grows during the dry
188 season and shrinks during the wet season (black line in Figure S2g). The maximum deficit each year (red dots, estimated
189 by October 1 deficit for all analyses for simplicity), provides information about how much water was removed from storage
190 during the preceding dry season(s) by ET. Note that the October 1 deficit is always larger than the soil water storage capacity,
191 indicating that plants access water stored in weathered bedrock. The minimum deficit each year (yellow dots) provides
192 information about wet season replenishment of root zone storage. For Ward Creek shown in Figure S2g, the minimum deficit is
193 always 0, but it can be nonzero and even grow across multiple years at other sites—see the data supplement for study sites that
194 demonstrate deficit carry-over between years (34). In 2021, a large deficit was generated—among the largest during the study
195 period. As with the other hypothesis variables, though, the significance of the 2021 deficit is much clearer when compared
196 to the annual water budget. Figure S2o shows that the deficit as a fraction of the annual precipitation was more than 50%
197 larger than the largest observed value in previous years. Thus, the deficit strongly identifies 2021 as an outlier, consistent with
198 observations of substantial missing streamflow, and the root zone storage deficit explains 51% of the variance in residuals in the
199 SWE-Q relationship at Ward Creek. At nearly all study sites, the October 1 deficit in 2021 was the largest or second-largest
200 deficit recorded in the study period (as a fraction of WY P). Some sites have R^2 values greater than 0.7, while others have
201 values less than 0.1, with a median of 0.32.

202 These exploratory analyses motivated the choice of variables included in the multiple linear regression model. The outcomes
203 of the multiple linear regression are summarized in Table S3 for (top) wet years and (bottom) dry years. Performance
204 comparison between different linear regression models is in Table S4.

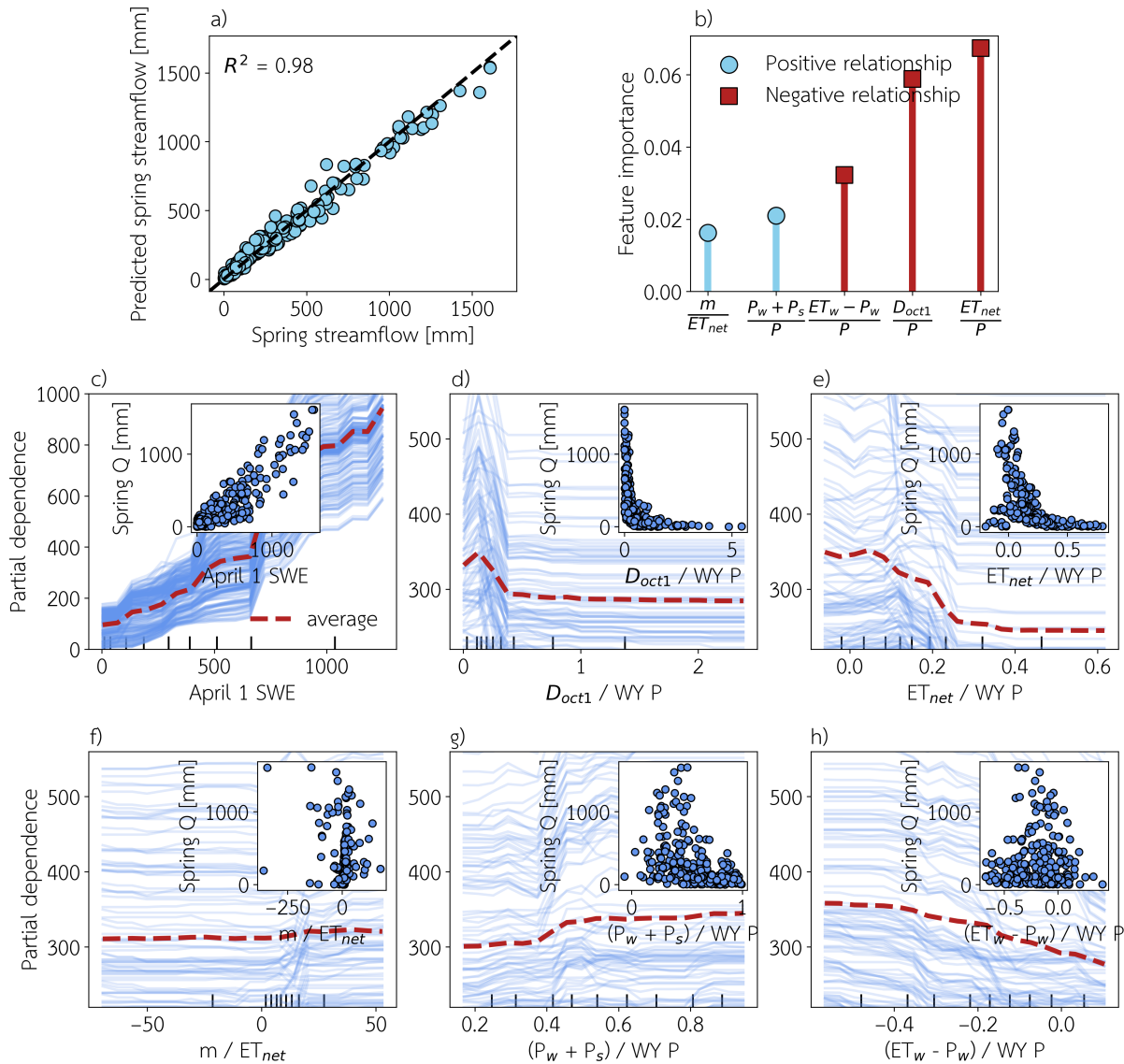


Fig. S3. (a) Performance of random forest model for spring streamflow trained for all study sites. (b) Feature importance for parameters included in random forest model, except for April 1 SWE, which is significantly more important than all other parameters. (c)-(h) are partial dependence plots with the average partial dependence shown as a red dashed line. Panels (d)-(e) are zoomed in, which excludes some of the blue lines but allows for the functional shape of the relationships to be more clearly seen. For comparison, scatter data for the relationship between each parameter and measured spring streamflow is shown as an inset to each subplot.

205 **A random forest model for spring streamflow**

206 In this study, we developed a multiple linear regression model for each study site to explain spring streamflow production from
 207 snowmelt. However, while the model presented in the main text shows linear relationships among all variables for idealized
 208 catchments, the relationships between each investigated variable may not be linear for real catchments. To capture more
 209 complex relationships among the variables, we also developed a random forest model, using the same set of variables described
 210 in Table 1 in the main text. Since random forest models are data-driven and flexible, we chose to train a single random forest
 211 model using data from all sites. Performance of the random forest model was exceptional (Figure S3a, $R^2 = 0.98$), and feature
 212 importance (Figure S3b) supports similar conclusions to the effect size results using the multiple linear regression model. The
 213 exact ordering of feature importance is not identical to the ordering implied by the multiple linear regression, but both models
 214 support the conclusion that the melt rate does not provide much predictive power, and the deficit provides a substantial
 215 amount of predictive power. Partial dependence plots (Figure S3c-h) shows the functional form of the learned relationship
 216 between each variable and the output (spring streamflow). These functional forms are nearly monotonic, with small deviations
 217 from monotonic behavior likely due to co-variability of variables with parameters not included in the model. In all cases, the
 218 general direction of the relationship matches our hypotheses in the main text: (c) higher SWE results in higher streamflow, (d)
 219 larger deficit results in smaller streamflow, (e) more spring ET results in less streamflow, (f) a faster melt rate results in more
 220 streamflow, (g) more rainfall results in more streamflow, and (h) less winter ET results in more streamflow. Insets show the

221 raw data used to train the model. For the most predictive variables, the learned relationship is clearly visible in scatter plots of
 222 raw data as well, providing additional confidence in the results.

223 **Including the deficit in a model for snowmelt runoff improves performance on under-predicted years**

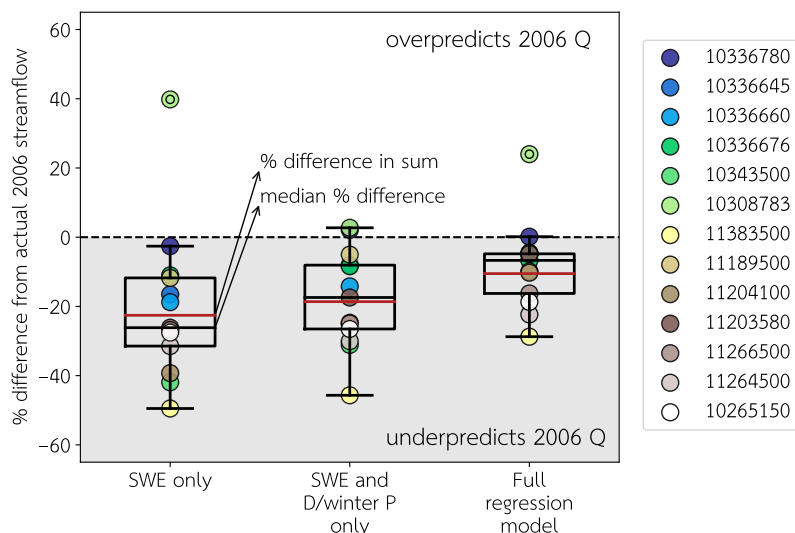


Fig. S4. Performance of regression models at 13 study sites for the year 2021. A linear regression model using only April 1 SWE underpredicts the total 2006 spring streamflow at all sites by 23% for total streamflow across all sites (median 26%), while the full linear regression model or a model using April 1 SWE and October deficit as a fraction of winter precipitation underpredicts the total by 19 or 11% (median of 17 or 7%), respectively.

224 In the main text, we explored the importance of the deficit for capturing snowmelt runoff on years with anomalously low
 225 runoff. Here, we explore the importance of the deficit for capturing snowmelt runoff on years with anomalously high runoff, such
 226 as 2006. Figure S4 demonstrates that including the deficit drastically reduces the extent to which streamflow is underpredicted
 227 from a median of 26% to 17%. While not as striking as the result for 2021, this difference is still important for management
 228 applications and demonstrates that the deficit can improve predictions for all anomalous years, not just overpredicted years.

229 **Including the deficit in a model for snowmelt runoff improves performance on larger, disturbed basins of economic
 230 importance**

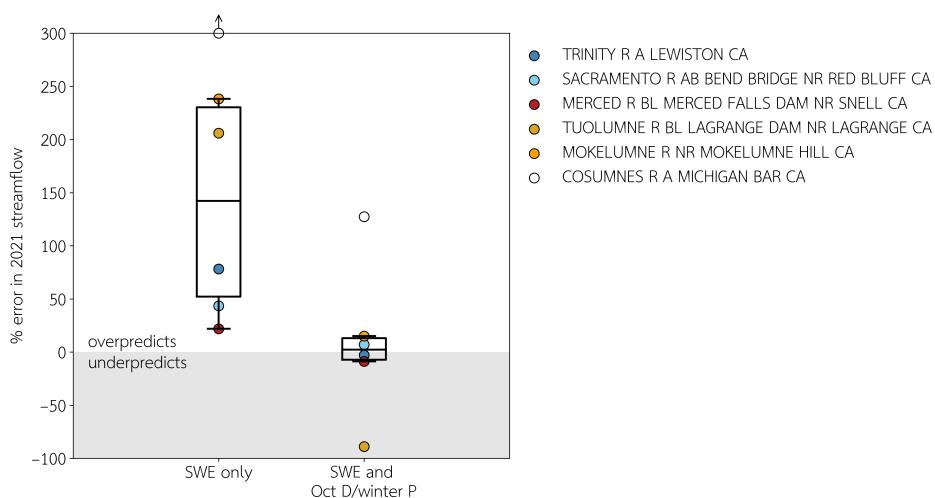


Fig. S5. Comparison of performance of a linear regression model based only on April 1 SWE and one using both April 1 SWE and October 1 Deficit / winter precipitation. Error is reduced from a median of 143% to 2%.

231 For this study, we selected a set of minimally disturbed watersheds to test our model. However, the basins where snowmelt
 232 runoff predictions matter for water supply are much larger, more complex, and more disturbed than the study sites. To

233 demonstrate that our model is still relevant to these basins, we tested whether adding October 1 Deficit to a linear model
234 for snowmelt runoff for these basins. The improvement in model performance applies also to these larger, more complex and
235 disturbed basins (Figure S5), reducing median model error from 143% to 2%. Outliers for Cosumnes and Tuolumne only appear
236 to have large percent error since the actual streamflow is very small.

237 References

- 238 1. Baird Langenbrunner, J David Neelin, Benjamin R Lintner, and Bruce T Anderson. Patterns of precipitation change and
239 climatological uncertainty among cmip5 models, with a focus on the midlatitude pacific storm track. *Journal of Climate*,
240 28(19):7857–7872, 2015.
- 241 2. Daniel E Horton, Nathaniel C Johnson, Deepti Singh, Daniel L Swain, Bala Rajaratnam, and Noah S Diffenbaugh.
242 Contribution of changes in atmospheric circulation patterns to extreme temperature trends. *Nature*, 522(7557):465–469,
243 2015.
- 244 3. Michael D Dettinger, Fred Martin Ralph, Tapash Das, Paul J Neiman, and Daniel R Cayan. Atmospheric rivers, floods
245 and the water resources of california. *Water*, 3(2):445–478, 2011.
- 246 4. Daniel L Swain, Baird Langenbrunner, J David Neelin, and Alex Hall. Increasing precipitation volatility in twenty-first-
247 century california. *Nature Climate Change*, 8(5):427–433, 2018.
- 248 5. Daniel Griffin and Kevin J Anchukaitis. How unusual is the 2012–2014 california drought? *Geophysical Research Letters*,
249 41(24):9017–9023, 2014.
- 250 6. Daniel L Swain, Daniel E Horton, Deepti Singh, and Noah S Diffenbaugh. Trends in atmospheric patterns conducive to
251 seasonal precipitation and temperature extremes in california. *Science Advances*, 2(4):e1501344, 2016.
- 252 7. Scott M Robeson. Revisiting the recent california drought as an extreme value. *Geophysical Research Letters*, 42(16):
253 6771–6779, 2015.
- 254 8. Scott L Stephens, Brandon M Collins, Christopher J Fettig, Mark A Finney, Chad M Hoffman, Eric E Knapp, Malcolm P
255 North, Hugh Safford, and Rebecca B Wayman. Drought, tree mortality, and wildfire in forests adapted to frequent fire.
256 *BioScience*, 68(2):77–88, 2018.
- 257 9. Noah S Diffenbaugh, Daniel L Swain, and Danielle Touma. Anthropogenic warming has increased drought risk in california.
258 *Proceedings of the National Academy of Sciences*, 112(13):3931–3936, 2015.
- 259 10. Christopher J Fettig, Leif A Mortenson, Beverly M Bulaon, and Patra B Foulk. Tree mortality following drought in the
260 central and southern sierra nevada, california, us. *Forest Ecology and Management*, 432:164–178, 2019.
- 261 11. Alejandro Guarín and Alan H Taylor. Drought triggered tree mortality in mixed conifer forests in yosemite national park,
262 california, usa. *Forest ecology and management*, 218(1-3):229–244, 2005.
- 263 12. Sarah Byer and Yufang Jin. Detecting drought-induced tree mortality in sierra nevada forests with time series of satellite
264 data. *Remote Sensing*, 9(9):929, 2017.
- 265 13. S-Y Simon Wang, Jin-Ho Yoon, Emily Becker, and Robert Gillies. California from drought to deluge. *Nature Climate*
266 *Change*, 7(7):465–468, 2017.
- 267 14. Alexander L Handwerker, Eric J Fielding, Mong-Han Huang, Georgina L Bennett, Cunren Liang, and William H Schulz.
268 Widespread initiation, reactivation, and acceleration of landslides in the northern california coast ranges due to extreme
269 rainfall. *Journal of Geophysical Research: Earth Surface*, 124(7):1782–1797, 2019.
- 270 15. U.S. Geological Survey. National water information system data available on the world wide web (water data for the
271 nation), 2021. accessed December 2021.
- 272 16. JA Falcone. Us geological survey gages-ii time series data from consistent sources of land use, water use, agriculture,
273 timber activities, dam removals, and other historical anthropogenic influences: Us geological survey data release. In *US*
274 *Geological Survey Data Release*. 2017.
- 275 17. ME Wiczorek. USGS Streamgage NHDPlus Version 1 Basins 2011, 2011.
- 276 18. Collin Homer, Jon Dewitz, Limin Yang, Suming Jin, Patrick Danielson, George Xian, John Coulston, Nathaniel Herold,
277 James Wickham, and Kevin Megown. Completion of the 2011 national land cover database for the conterminous united
278 states—representing a decade of land cover change information. *Photogrammetric Engineering & Remote Sensing*, 81(5):
279 345–354, 2015.
- 280 19. State of California and the Department of Forestry and Fire Protection. Fire perimeters through 2020, 2021.
- 281 20. CAL FIRE. Timber harvest plans (THPs) - CAL FIRE [ds816], 2019.
- 282 21. W Jesse Hahm, DN Dralle, DM Rempe, AB Bryk, SE Thompson, TE Dawson, and WE Dietrich. Low subsurface
283 water storage capacity relative to annual rainfall decouples mediterranean plant productivity and water use from rainfall
284 variability. *Geophysical Research Letters*, 46(12):6544–6553, 2019.
- 285 22. Michael L Goulden and Roger C Bales. California forest die-off linked to multi-year deep soil drying in 2012–2015 drought.
286 *Nature Geoscience*, 12(8):632–637, 2019.
- 287 23. W Jesse Hahm, David N Dralle, Maryn Sanders, Alexander B Bryk, Kristen Elizabeth Fauria, Mong-Han Huang, Berit
288 Hudson-Rasmussen, Mariel D Nelson, Michelle A Pedrazas, Logan Marcos Schmidt, et al. Bedrock vadose zone storage
289 dynamics under extreme drought: consequences for plant water availability, recharge, and runoff. *ESSOAR Pre-Print*
290 (<https://www.essoar.org/doi/abs/10.1002/essoar.10509661.2>), 2021.
- 291 24. Erica L McCormick, David N Dralle, W Jesse Hahm, Alison K Tune, Logan M Schmidt, K Dana Chadwick, and Daniella M
292 Rempe. Widespread woody plant use of water stored in bedrock. *Nature*, 597(7875):225–229, 2021.

- 293 25. Lan Wang-Erlandsson, Wim GM Bastiaanssen, Hongkai Gao, Jonas Jägermeyr, Gabriel B Senay, Albert IJM Van Dijk,
294 Juan P Guerschman, Patrick W Keys, Line J Gordon, and Hubert HG Savenije. Global root zone storage capacity from
295 satellite-based evaporation. *Hydrology and Earth System Sciences*, 20(4):1459–1481, 2016.
- 296 26. Guotao Cui, Qin Ma, and Roger Bales. Assessing multi-year-drought vulnerability in dense mediterranean-climate forests
297 using water-balance-based indicators. *Journal of Hydrology*, page 127431, 2022.
- 298 27. Keirnan Fowler, Wouter Knoben, Murray Peel, Tim Peterson, Dongryeol Ryu, Margarita Saft, Ki-Weon Seo, and Andrew
299 Western. Many commonly used rainfall-runoff models lack long, slow dynamics: Implications for runoff projections. *Water
300 Resources Research*, 56(5):e2019WR025286, 2020.
- 301 28. Tim J Peterson, M Saft, MC Peel, and A John. Watersheds may not recover from drought. *Science*, 372(6543):745–749,
302 2021.
- 303 29. David N Dralle, W Jesse Hahm, K Dana Chadwick, Erica McCormick, and Daniella M Rempe. Accounting for snow in
304 the estimation of root zone water storage capacity from precipitation and evapotranspiration fluxes. *Hydrology and Earth
305 System Sciences*, 25(5):2861–2867, 2021.
- 306 30. National Operational Hydrologic Remote Sensing Center. Snow data assimilation system (snodas) data products at nsidc,
307 version 1, 2000.
- 308 31. Gianluca Botter, Amilcare Porporato, Edoardo Daly, Ignacio Rodriguez-Iturbe, and Andrea Rinaldo. Probabilistic
309 characterization of base flows in river basins: Roles of soil, vegetation, and geomorphology. *Water Resources Research*, 43
310 (6), 2007.
- 311 32. Ignacio Rodriguez-Iturbe, Amilcare Porporato, Luca Ridolfi, V Isham, and DR Coxi. Probabilistic modelling of water
312 balance at a point: the role of climate, soil and vegetation. *Proceedings of the Royal Society of London. Series A:
313 Mathematical, Physical and Engineering Sciences*, 455(1990):3789–3805, 1999.
- 314 33. Carolyn T Hunsaker, Thomas W Whitaker, and Roger C Bales. Snowmelt runoff and water yield along elevation and
315 temperature gradients in california’s southern sierra nevada 1. *JAWRA Journal of the American Water Resources
316 Association*, 48(4):667–678, 2012.
- 317 34. Dana A Lapides, W Jesse Hahm, Daniella M Rempe, and David N Dralle. Supplementary code and data for: Root zone
318 storage deficits mediate the production of streamflow from snowmelt, 2021. accessed at [https://github.com/lapidesd/CA_](https://github.com/lapidesd/CA_missing_freshet)
319 [missing_freshet](https://github.com/lapidesd/CA_missing_freshet).